Supporting Information for:

Augmented Polyhydrazone Formation in Water by Template-Assisted Polymerization using Dual-Purpose Supramolecular Templates

Kai Zheng,[a†] Chang He,[a†] Hany F Nour,[a,b] Zhao Zhang,[a] Tianyu Yuan,[a,c] Hassan Traboulsi,[d] Javed Mazher,[d] Ali Trabolsi,[e] Lei Fang,[c] and Mark A. Olson*[a]

[a]*Institute for Molecular Design and Synthesis, School of Pharmaceutical Science and Technology, Tianjin University, 92 Weijin Road, Nankai District, Tianjin, P.R. China.*
[b]*National Research Centre, Photochemistry Department, Chemical Industries Research Division, 33 El Buhouth Street, P.O. Box 12622, Giza, Egypt.*
[c]*Department of Chemistry and Department of Materials Science and Engineering Department, Texas A&M University, 3003 TAMU, College Station, TX, USA.*
[d]*Chemistry Department and Physics Department, King Faisal University, Al Ahsa 31982, Kingdom of Saudi Arabia.*
[e]*Chemistry Program, New York University Abu Dhabi (NYUAD), Experimental Research Building (C1), Saadiyat Island, United Arab Emirates.*
[†]*Authors contributed equally to this work*

Table of Contents

1. NMR Spectroscopic Characterization

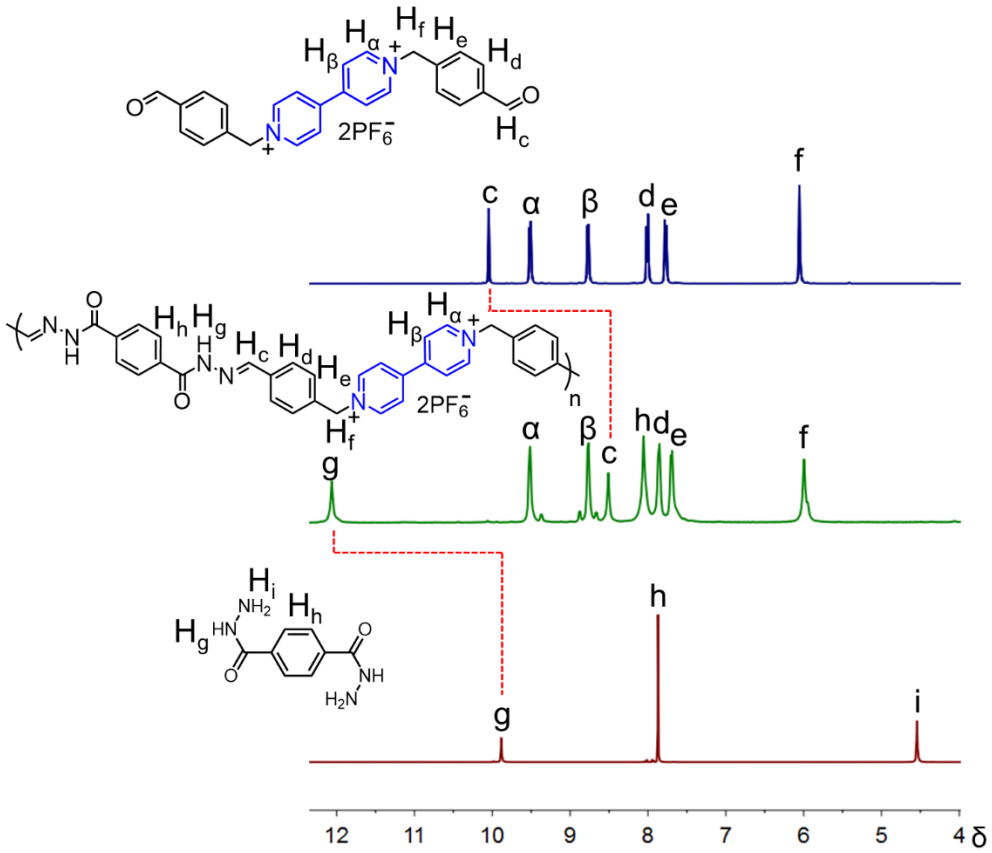

Figure S1. Stacked ^{1}H-NMR spectra of **1**·2PF$_6$ (top), polyhydrazone **3**·n2PF$_6$ (middle), and dihydrazide **2** (bottom) in DMSO-d_6 at 298 K.

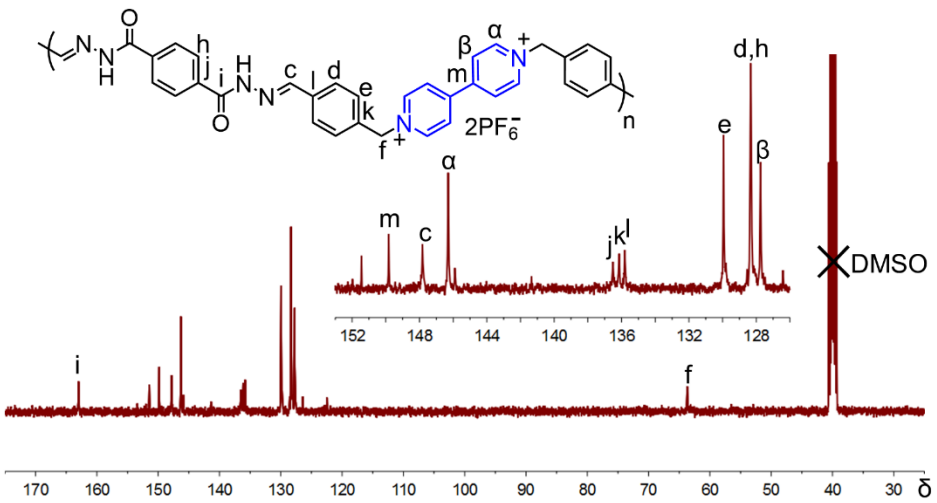

Figure S2. ^{13}C-NMR spectrum of polyhydrazone **3**·n2PF$_6$ in DMSO-d_6 at 298 K.

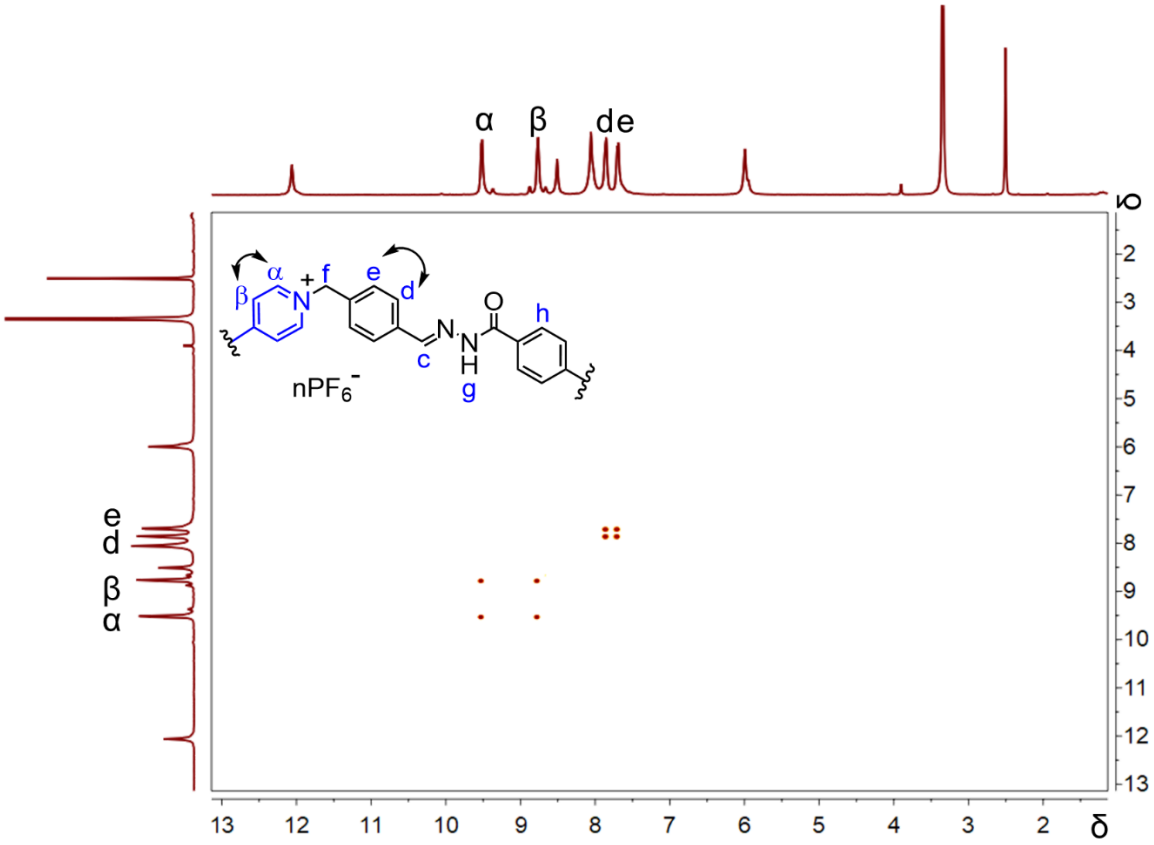

Figure S3. COSY spectrum of polyhydrazone **3**·n2PF_6 in DMSO-d_6 at 298 K.

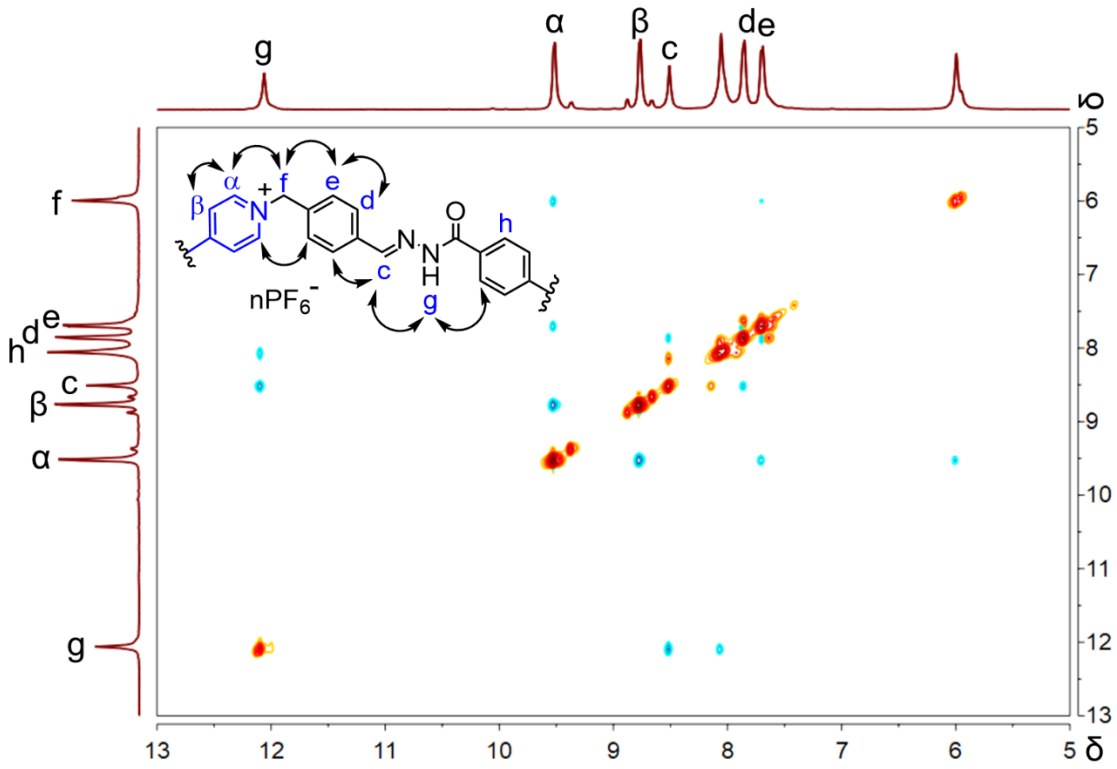

Figure S4. ROESY spectrum of polyhydrazone **3**·n2PF_6 in DMSO-d_6 at 298 K.

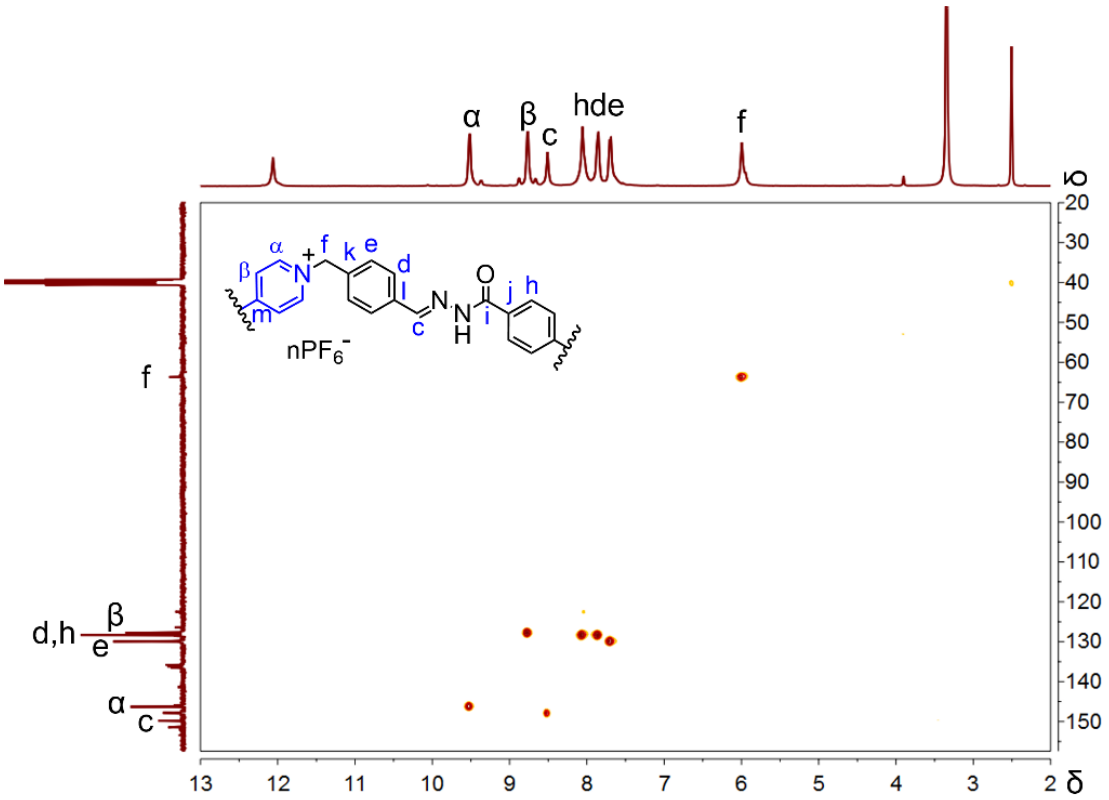

Figure S5. HSQC spectrum of polyhydrazone **3**·n2PF_6 in DMSO-d_6 at 298 K.

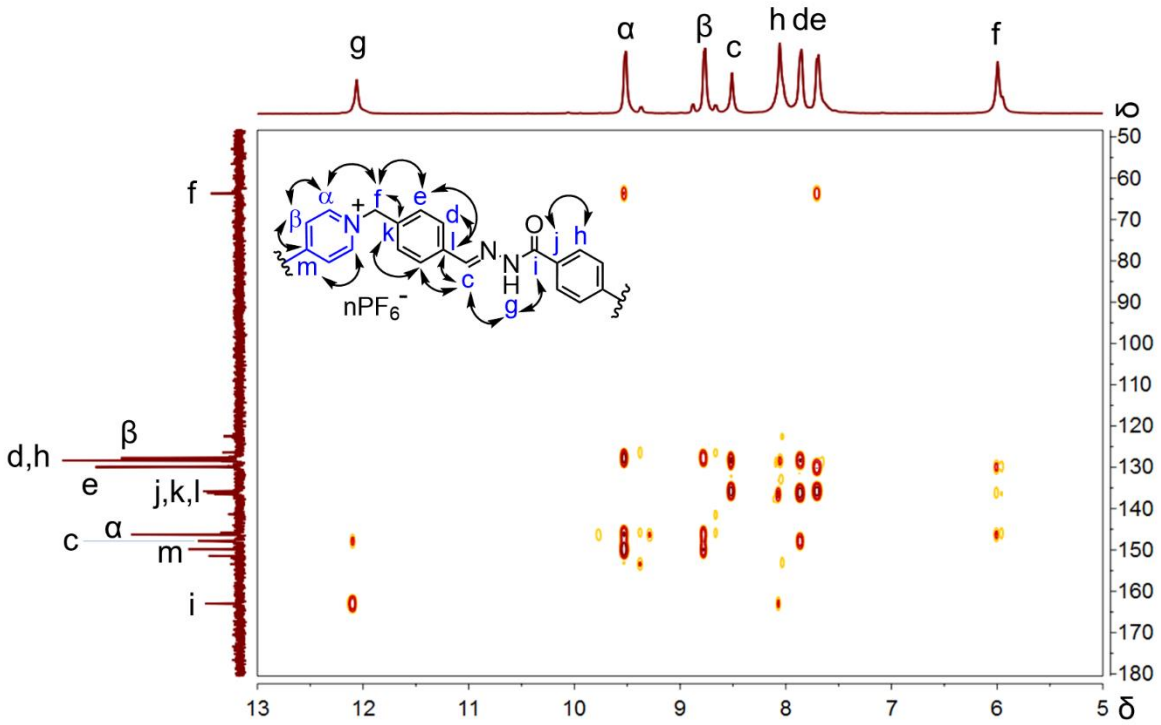

Figure S6. HMBC spectrum of polyhydrazone **3**·n2PF_6 in DMSO-d_6 at 298 K.

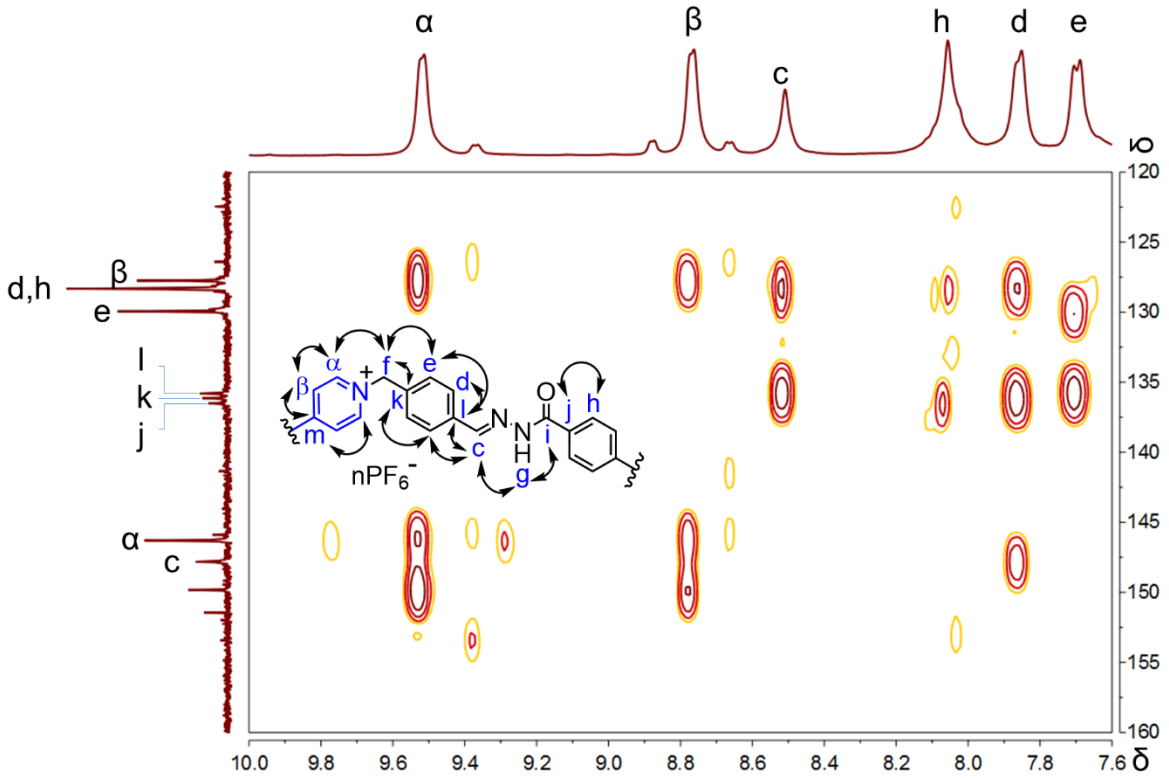

Figure S7. HMBC (zoomed) spectrum of polyhydrazone **3**·n2PF_6 in DMSO-d_6 at 298 K.

Table S1. 2D-NMR Correlations Measured for 3·n2PF_6

Spectra	Correlations
^{1}H-^{1}H COSY	H_e-H_d, H_α-H_β
^{1}H-^{1}H ROESY	H_e-H_f, H_α-H_f, H_α-H_e, H_c-H_d, H_g-H_h, H_g-H_c, H_α-H_β,
HMBC	H_e-C_f (^3J), H_α-C_f (^3J), H_f-C_e (^3J), H_f-C_α (^3J), H_f-C_k (^2J), H_g-C_c (^3J), H_g-C_i (^2J), H_α-C_β (^2J), H_β-C_β (^1J), H_c-C_d (^3J), H_d-C_d (^1J), H_e-C_e (^1J), H_e-C_l (^3J), H_d-C_k (^3J), H_h-C_j (^2J), H_c-C_l (^2J), H_β-C_α (^2J), H_α-C_β (^2J), H_β-C_m (^2J), H_α-C_m (^3J), H_d-C_c (^3J)
HSQC	H_α-C_α, H_β-C_β, H_c-C_c, H_d-C_d, H_e-C_e, H_f-C_f, H_h-C_h,

2. Molecular Recognition of Dialdehyde **1**·2Br with Molecular Templates

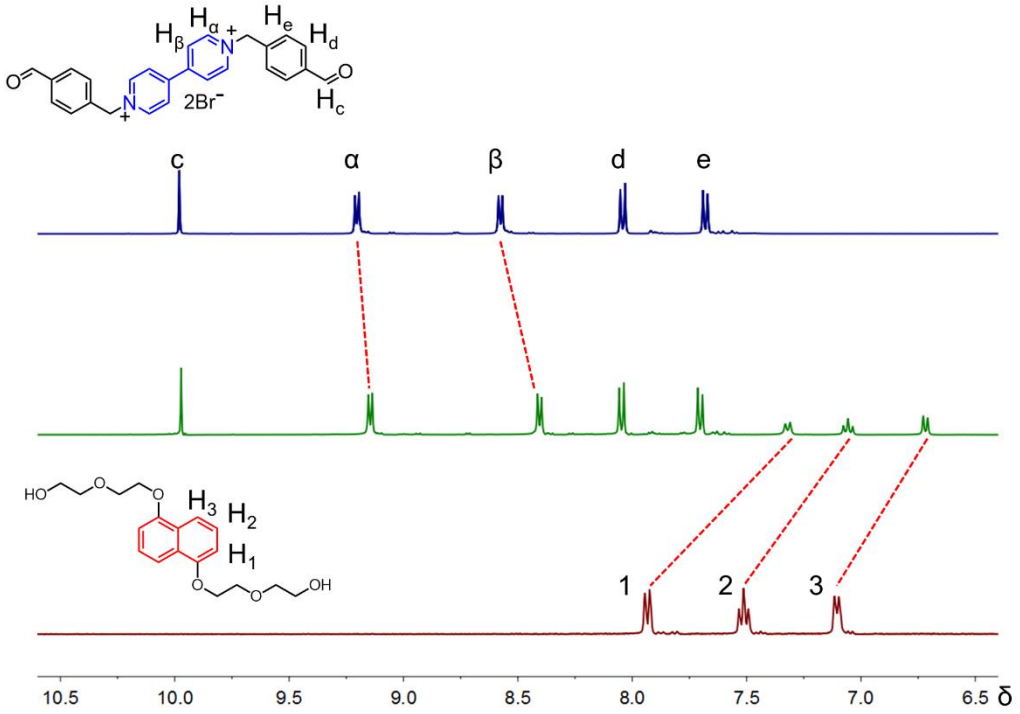

Figure S8. Stacked ^{1}H-NMR spectra of **1**·2Br (top), 1:1 equivalent mixture of **1**·2Br and **4** (middle), and template **4** (bottom) in D_2O at 298 K at 5×10^{-3} M.

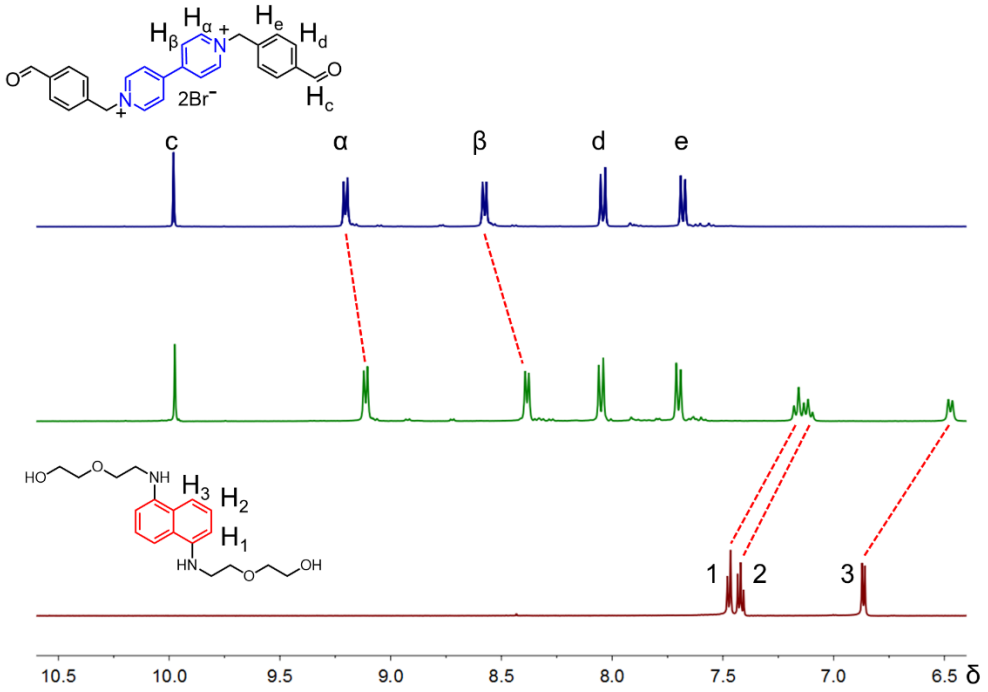

Figure S9. Stacked ^{1}H-NMR spectra of **1**·2Br (top), 1:1 equivalent mixture of **1**·2Br and **5** (middle), and template **5** (bottom) in D_2O at 298 K at 5×10^{-3} M.

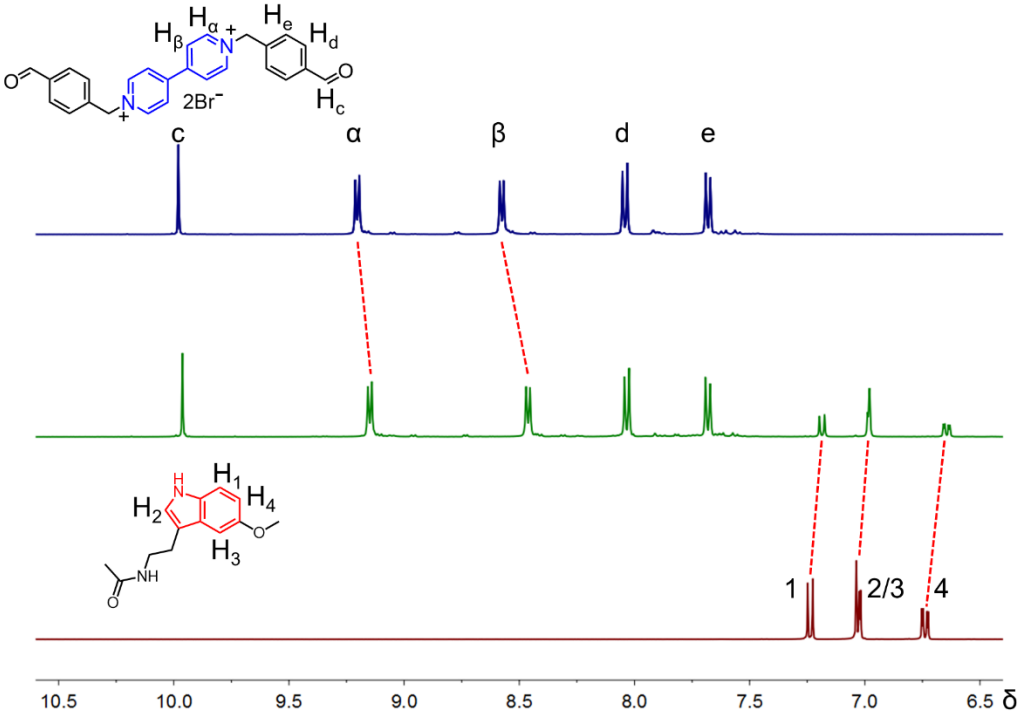

Figure S10. Stacked ^{1}H-NMR spectra of **1**·2Br (top), 1:1 equivalent mixture of **1**·2Br and **6** (middle), and template **6** (bottom) in D_2O at 298 K at 5×10^{-3} M.

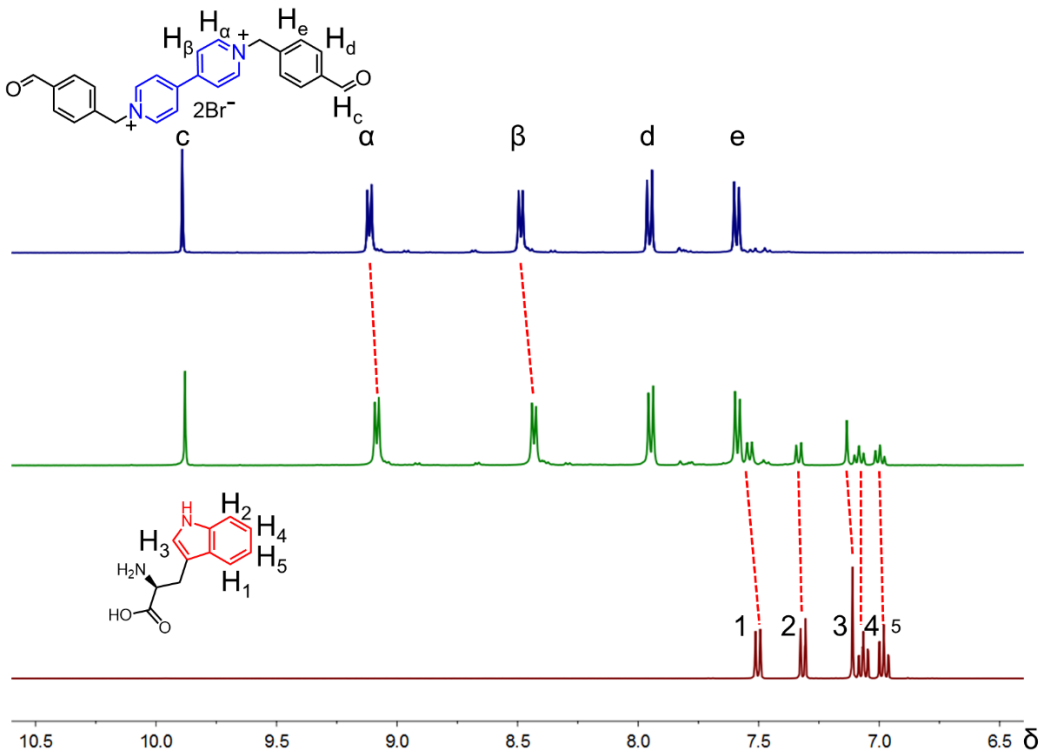

Figure S11. Stacked ^{1}H-NMR spectra of **1**·2Br (top), 1:1 equivalent mixture of **1**·2Br and **7** (middle), and template **7** (bottom) in D_2O at 298 K at 5×10^{-3} M.

3. GPC Data of polymer-nPF$_6$

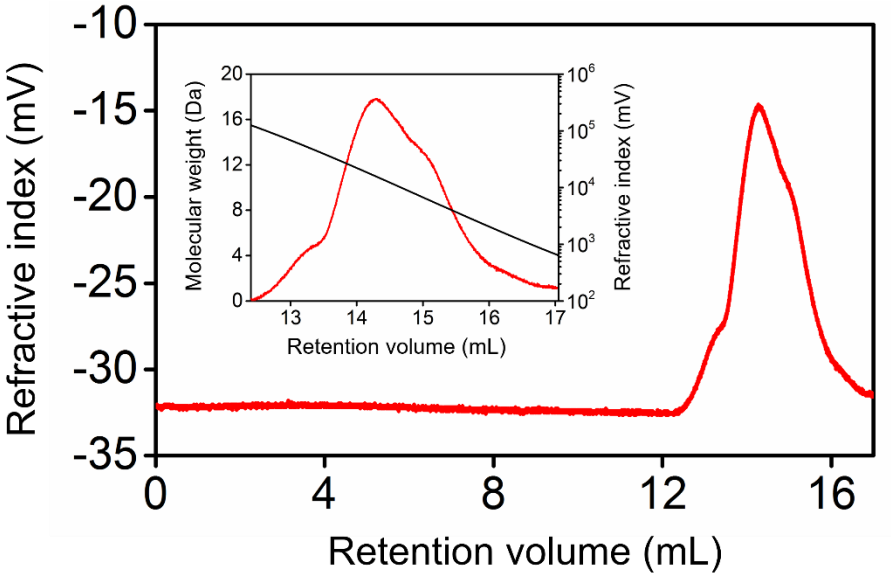

Peak RV (mL)	M_n (g·mol^{-1})	M_w (g·mol^{-1})	M_z (g·mol^{-1})	M_p (g·mol^{-1})	M_w/M_n
14.288	6,500	16,900	33,300	15,800	2.59

Figure S12. GPC analysis of **3**·n2PF$_6$.

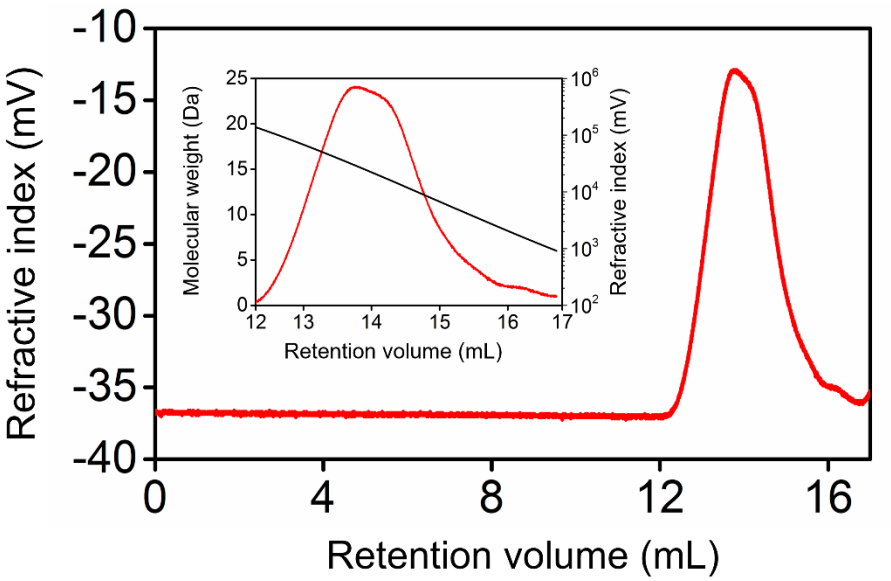

Peak RV (mL)	M_n (g·mol^{-1})	M_w (g·mol^{-1})	M_z (g·mol^{-1})	M_p (g·mol^{-1})	M_w/M_n
13.781	11,900	28,400	46,400	28,500	2.38

Figure S13. GPC analysis of **3**·n2PF$_6$ prepared by templation with **4**.

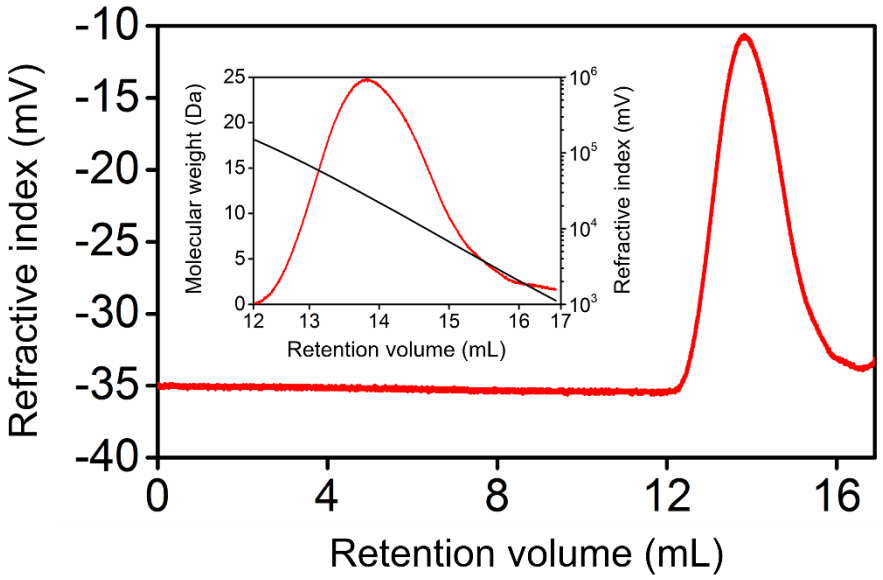

Peak RV (mL)	M_n (g·mol^{-1})	M_w (g·mol^{-1})	M_z (g·mol^{-1})	M_p (g·mol^{-1})	M_w/M_n
13.816	12,000	28,400	46,400	27,300	2.36

Figure S14. GPC analysis of **3**·n2PF$_6$ prepared by templation with **5.**

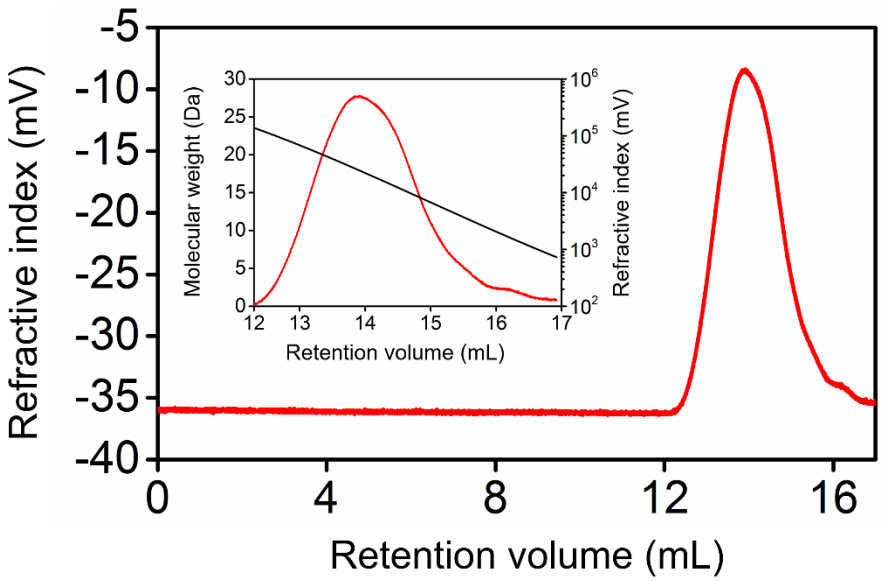

Peak RV (mL)	M_n (g·mol^{-1})	M_w (g·mol^{-1})	M_z (g·mol^{-1})	M_p (g·mol^{-1})	M_w/M_n
13.901	11,000	26,500	43,600	24,800	2.41

Figure S15. GPC analysis of **3**·n2PF$_6$ prepared by templation with **6**.

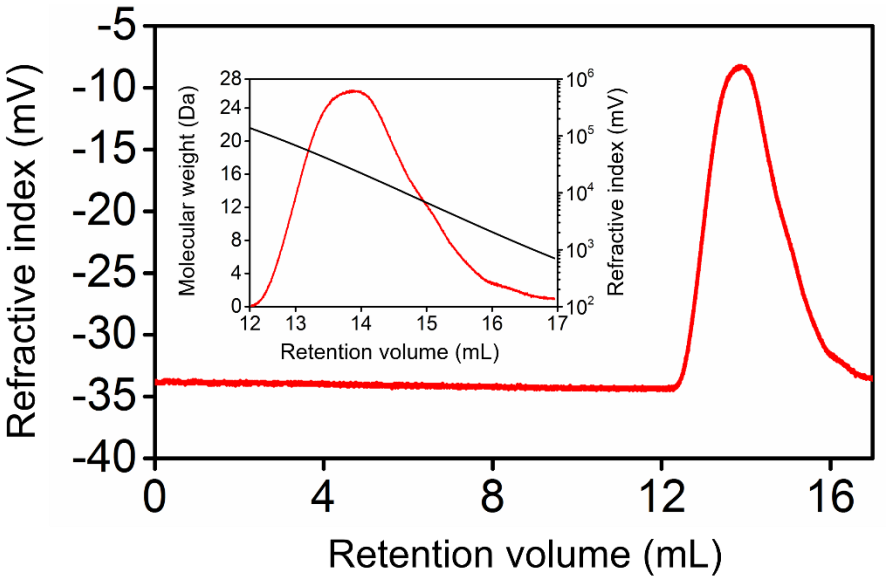

Peak RV (mL)	M_n (g·mol^{-1})	M_w (g·mol^{-1})	M_z (g·mol^{-1})	M_p (g·mol^{-1})	M_w/M_n
13.893	10,400	27,400	45,200	25,000	2.64

Figure S16. GPC analysis of **3**·n2PF$_6$ prepared by templation with **7**.

4. IR spectra of aerogels.

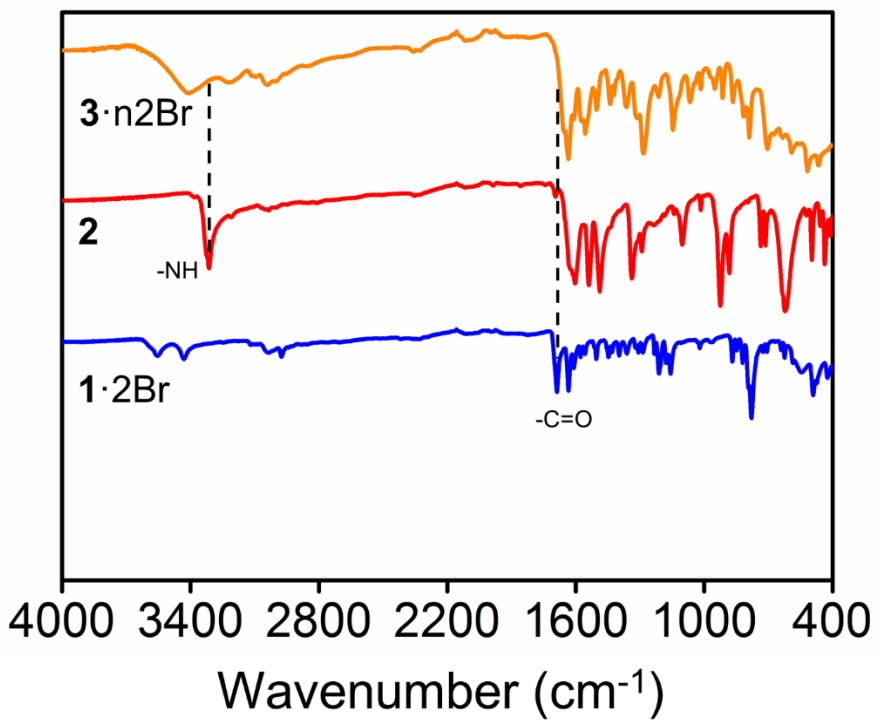

Figure S17. Stacked IR spectra of aerogel **3**·n2Br (top) and its precursors dihydrazide **2** (middle) and **1**·2Br (bottom).

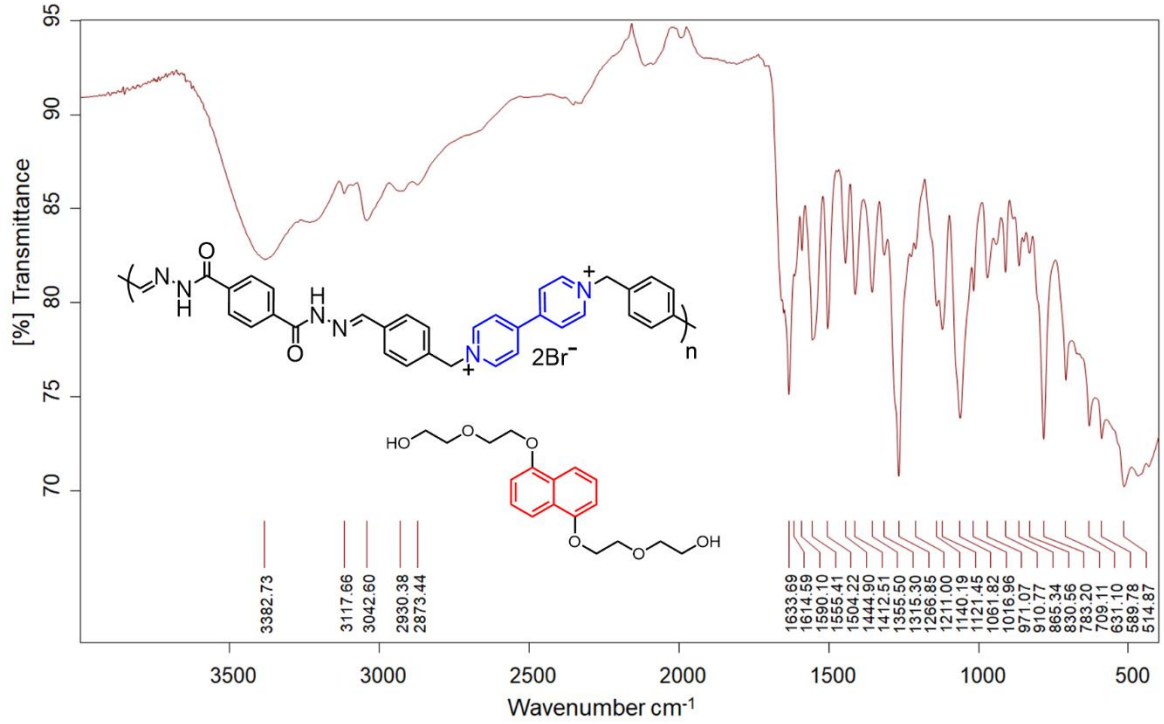

Figure S18. IR spectrum of aerogel **3**·n2Br⊃**4**

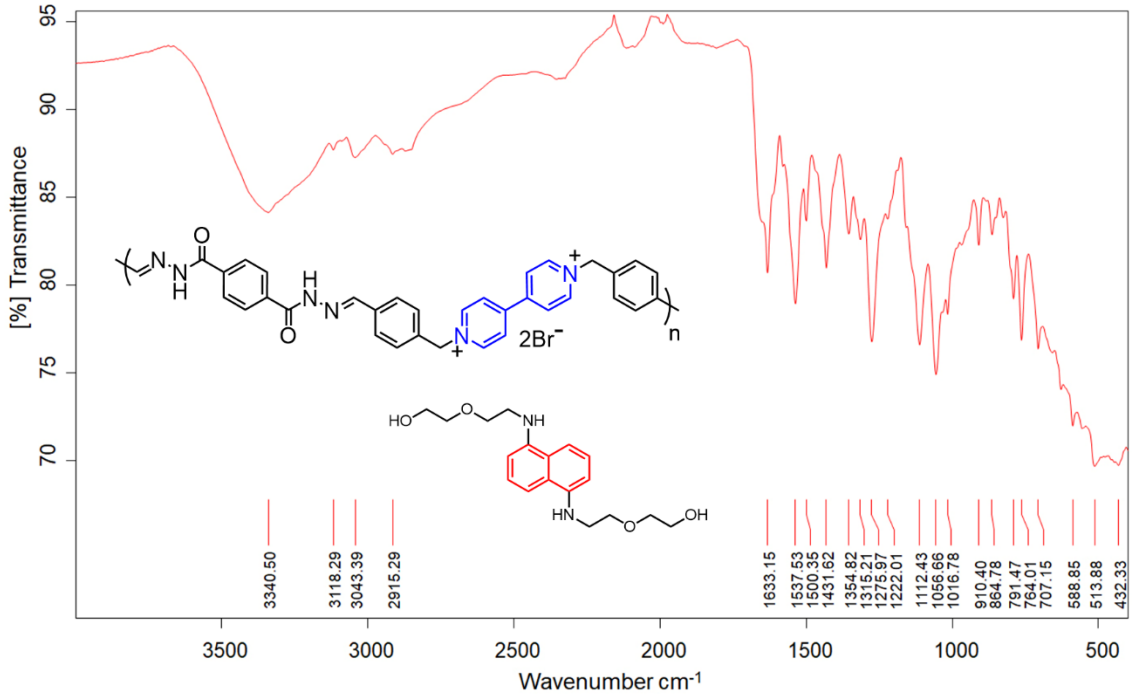

Figure S19. IR spectrum of aerogel **3**·n2Br⊃**5**.

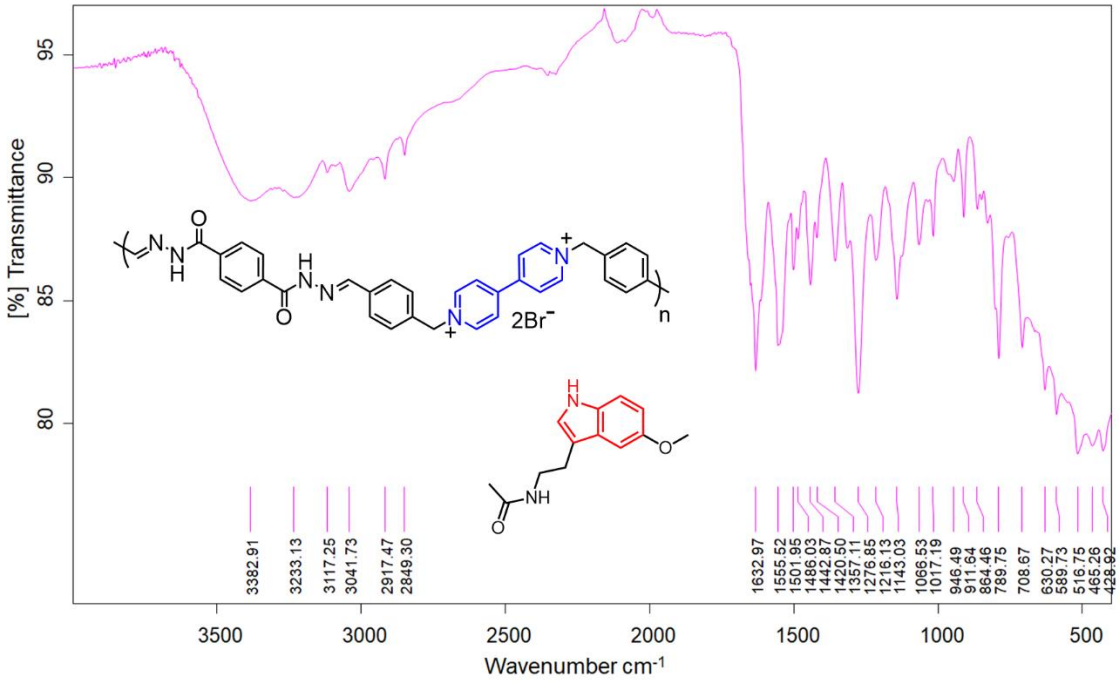

Figure S20. IR spectrum of aerogel **3**·n2Br⊃**6**.

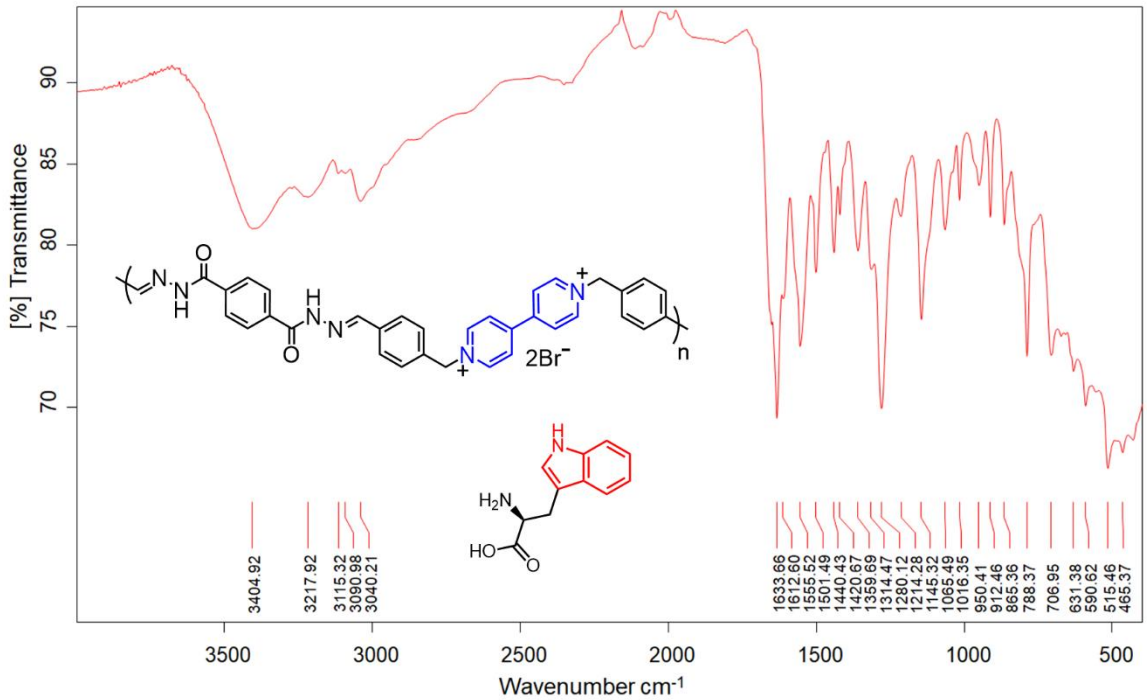

Figure S21. IR spectrum of aerogel **3**·n2Br⊃**7**

6. Competitive Hydrogen Bonding Urea Tests

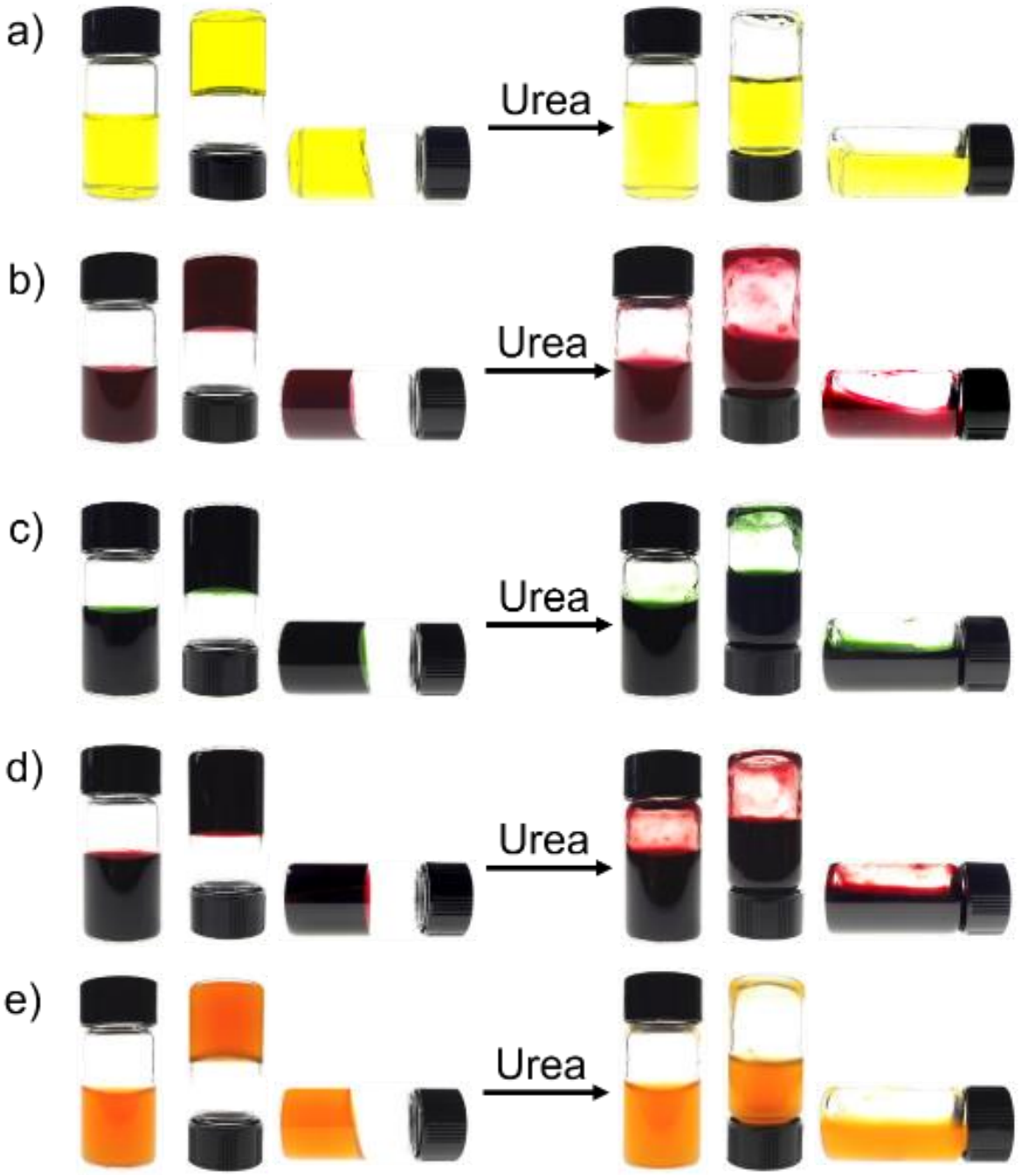

Figure S22. Competitive hydrogen bonding urea tests performed on (a) **3**·n2Br, (b) **3**·n2Br⊃**4**, (c) **3**·n2Br⊃**5**, (d) **3**·n2Br⊃**6**, and (e) **3**·n2Br⊃**7**-based hydrogels.

7. Rheological Properties of Untemplated and Templated Hydrogels.

7.1 Oscillatory Amplitude Stress Plots

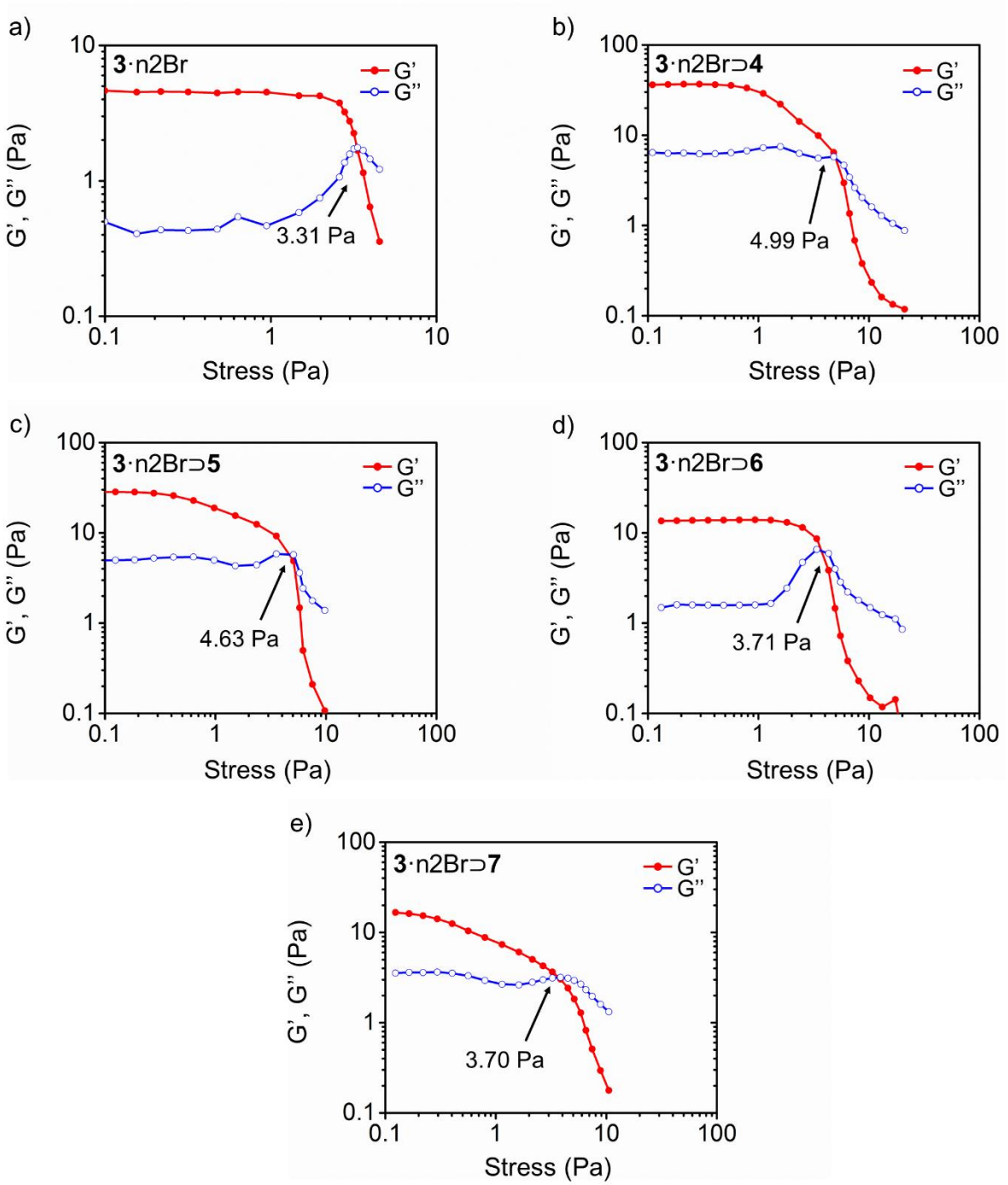

Figure S23. Oscillatory amplitude stress plots measured at a constant frequency of 1 Hz of the (a) untemplated and (b-e) templated hydrogels of **3**·n2Br prepared using a monomer concentration of 4 mM.

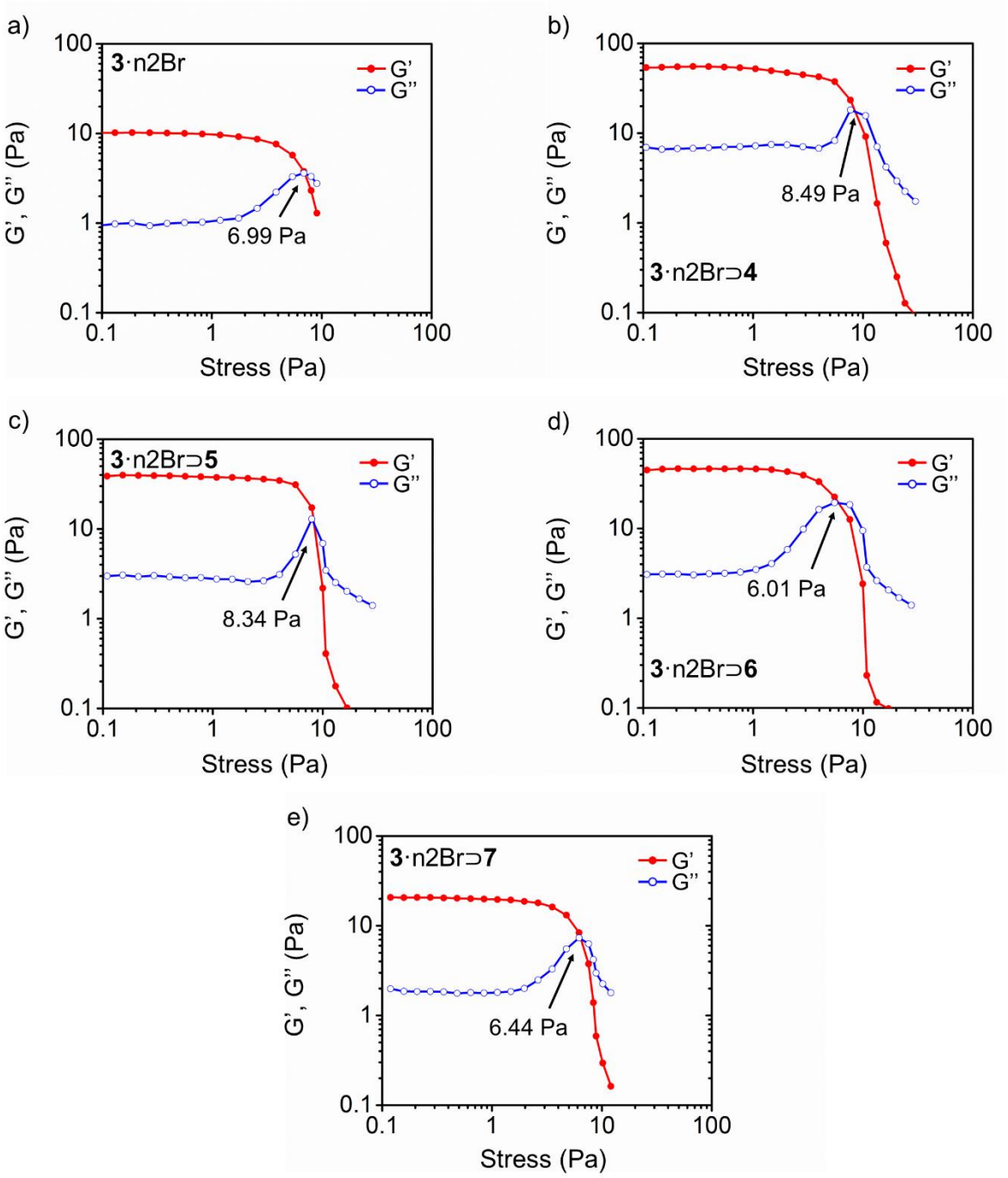

Figure S24. Oscillatory amplitude stress plots measured at a constant frequency of 1 Hz of the (a) untemplated and (b-e) templated hydrogels of **3**·n2Br prepared using a monomer concentration of 6 mM.

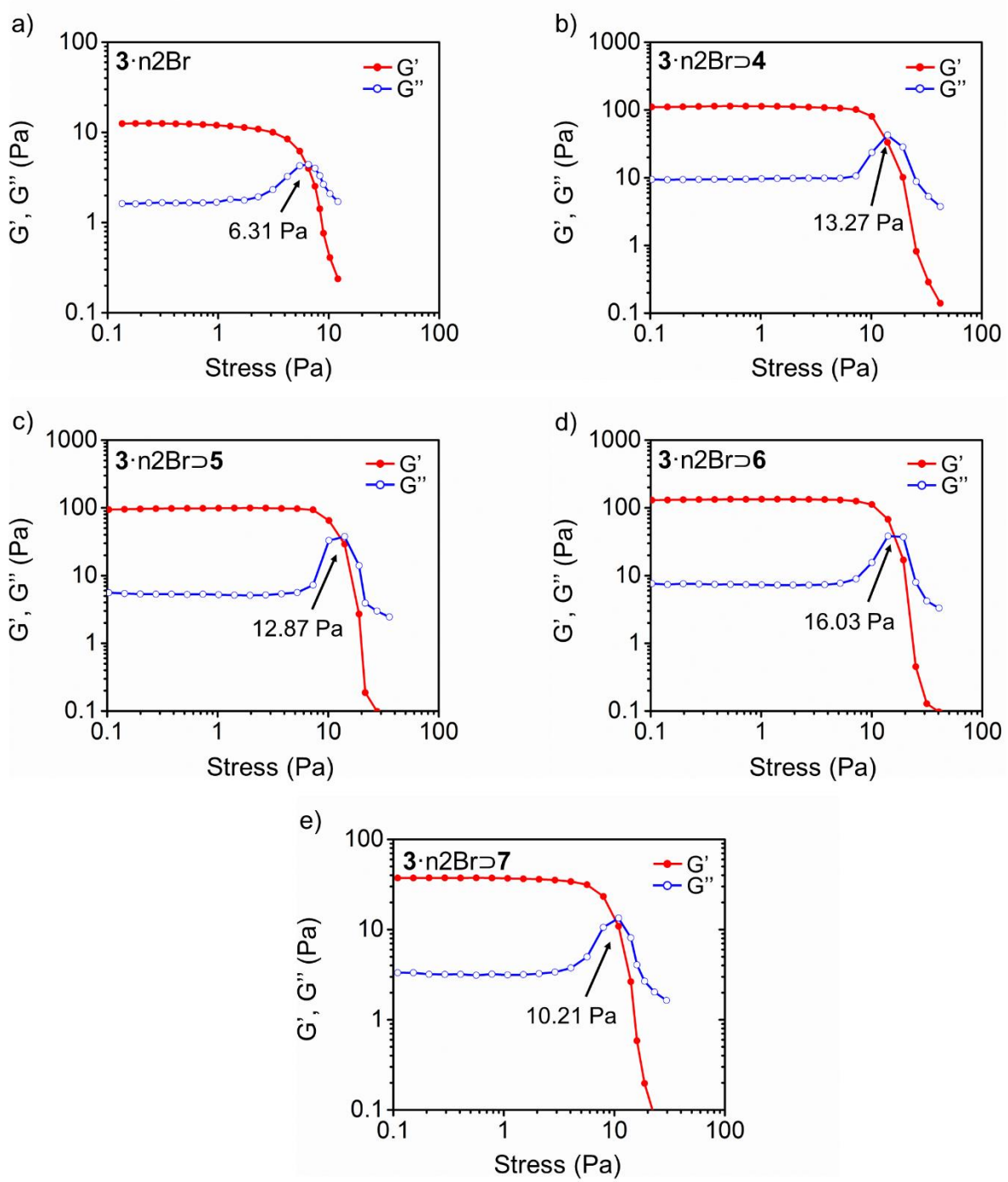

Figure S25. Oscillatory amplitude stress plots measured at a constant frequency of 1 Hz of the (a) untemplated and (b-e) templated hydrogels of **3**·n2Br prepared using a monomer concentration of 8 mM.

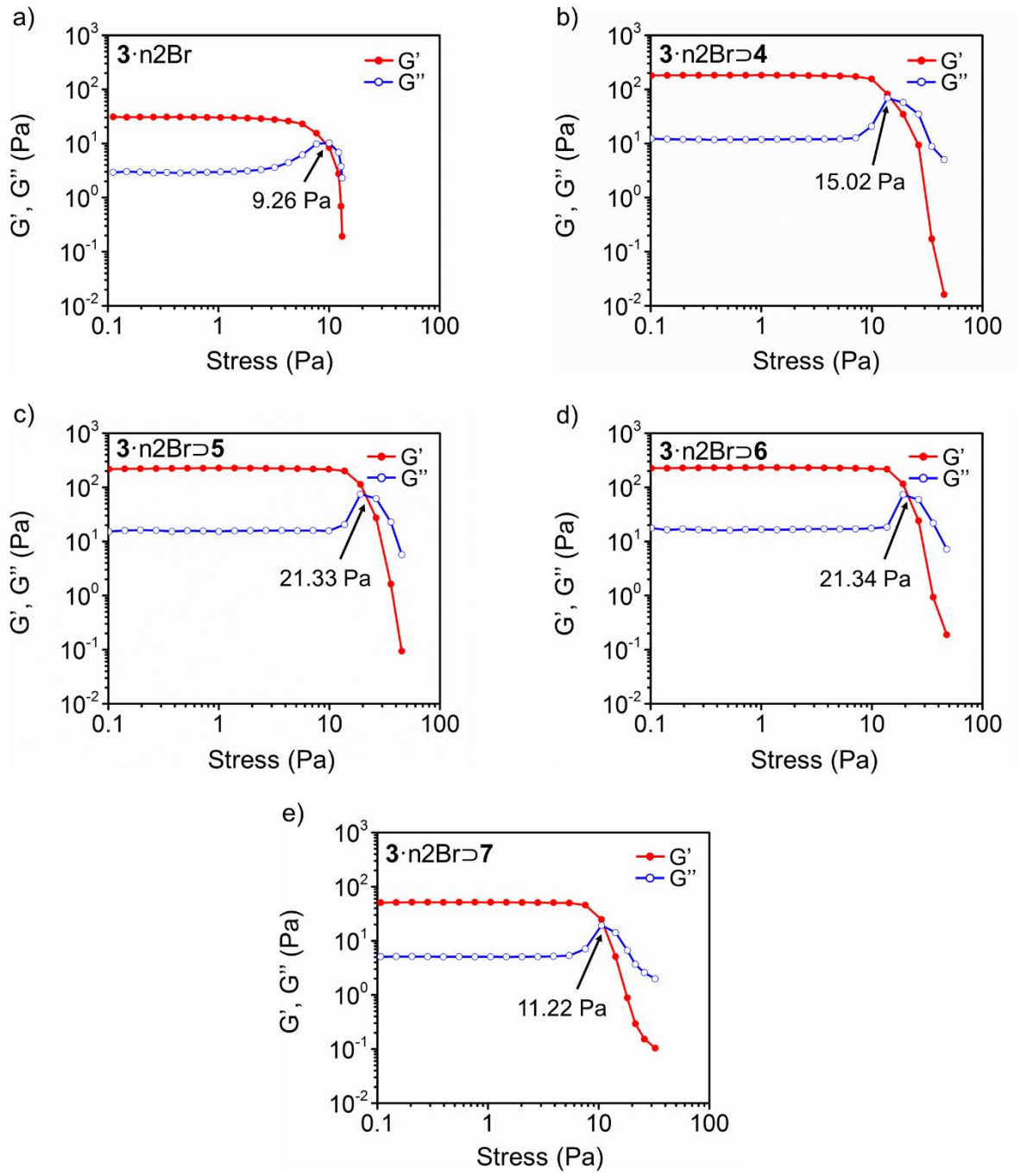

Figure S26. Oscillatory amplitude stress plots measured at a constant frequency of 1 Hz of the (a) untemplated and (b-e) templated hydrogels of **3**·n2Br prepared using a monomer concentration of 10 mM.

7.2 Oscillation Frequency Sweep Plots

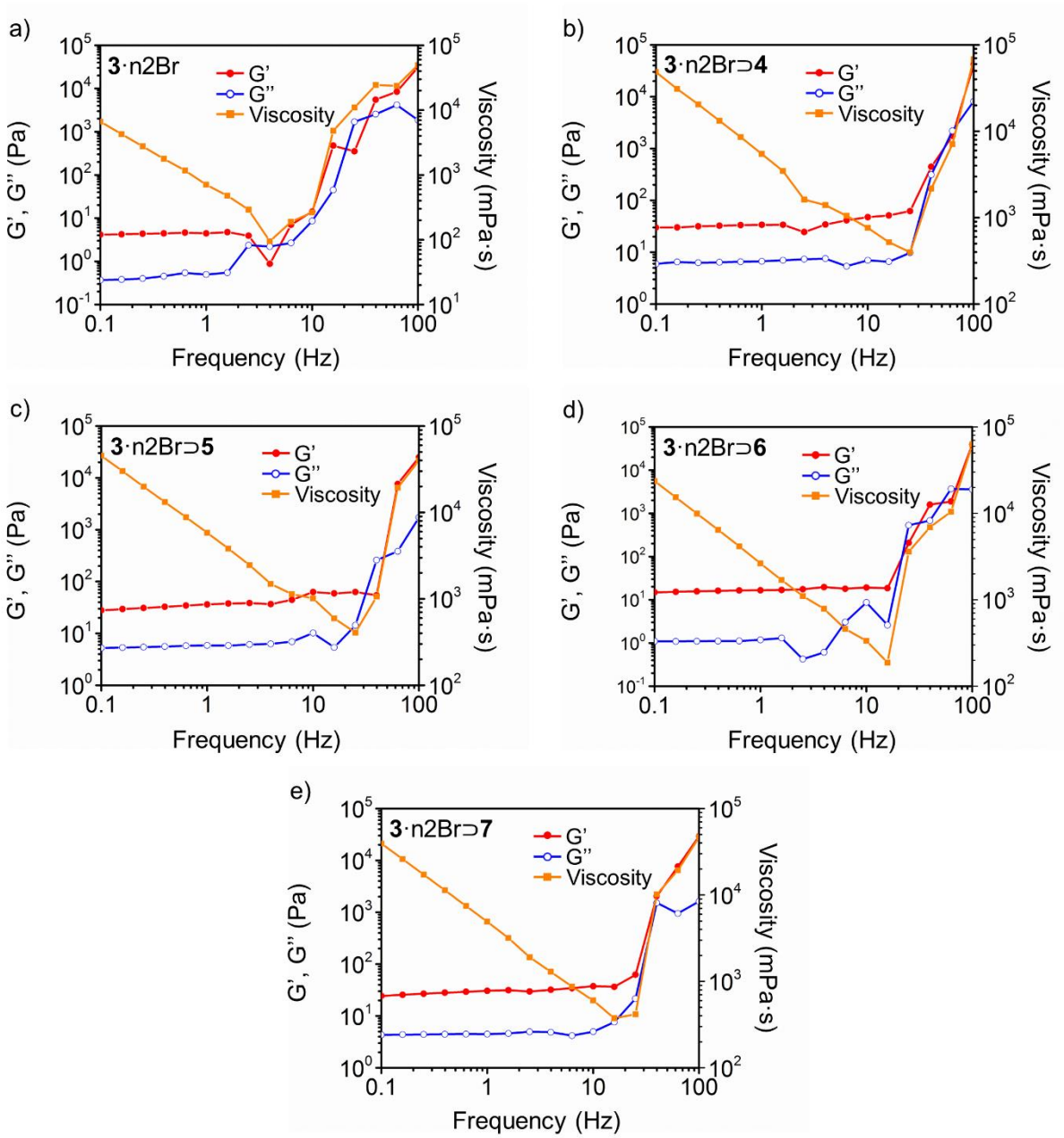

Figure S27. Oscillation frequency sweep plots of the (a) untemplated and (b-e) templated hydrogels of **3**·n2Br prepared using a monomer concentration of 4 mM.

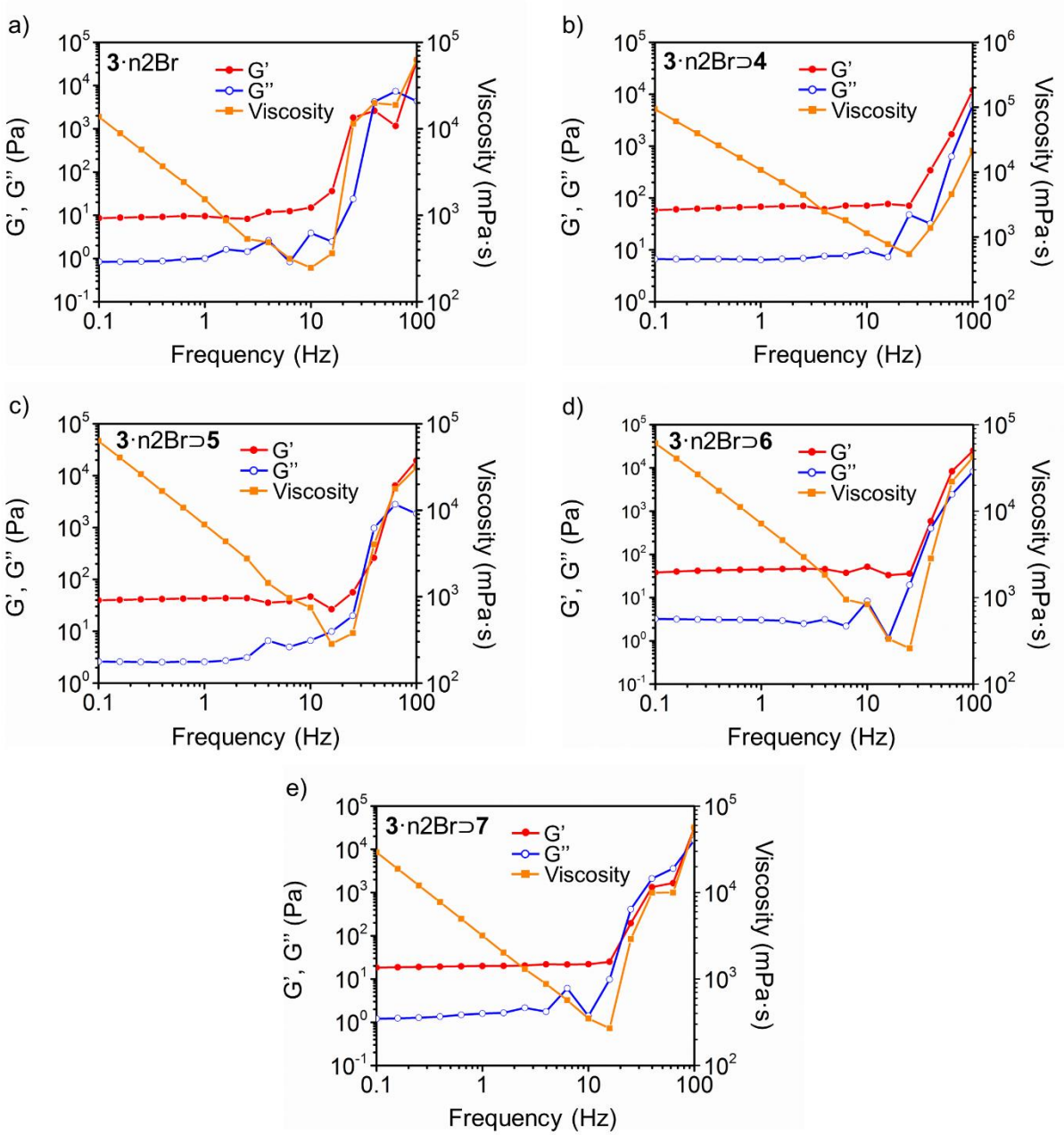

Figure S28. Oscillation frequency sweep plots of the (a) untemplated and (b-e) templated hydrogels of **3**·n2Br prepared using a monomer concentration of 6 mM.

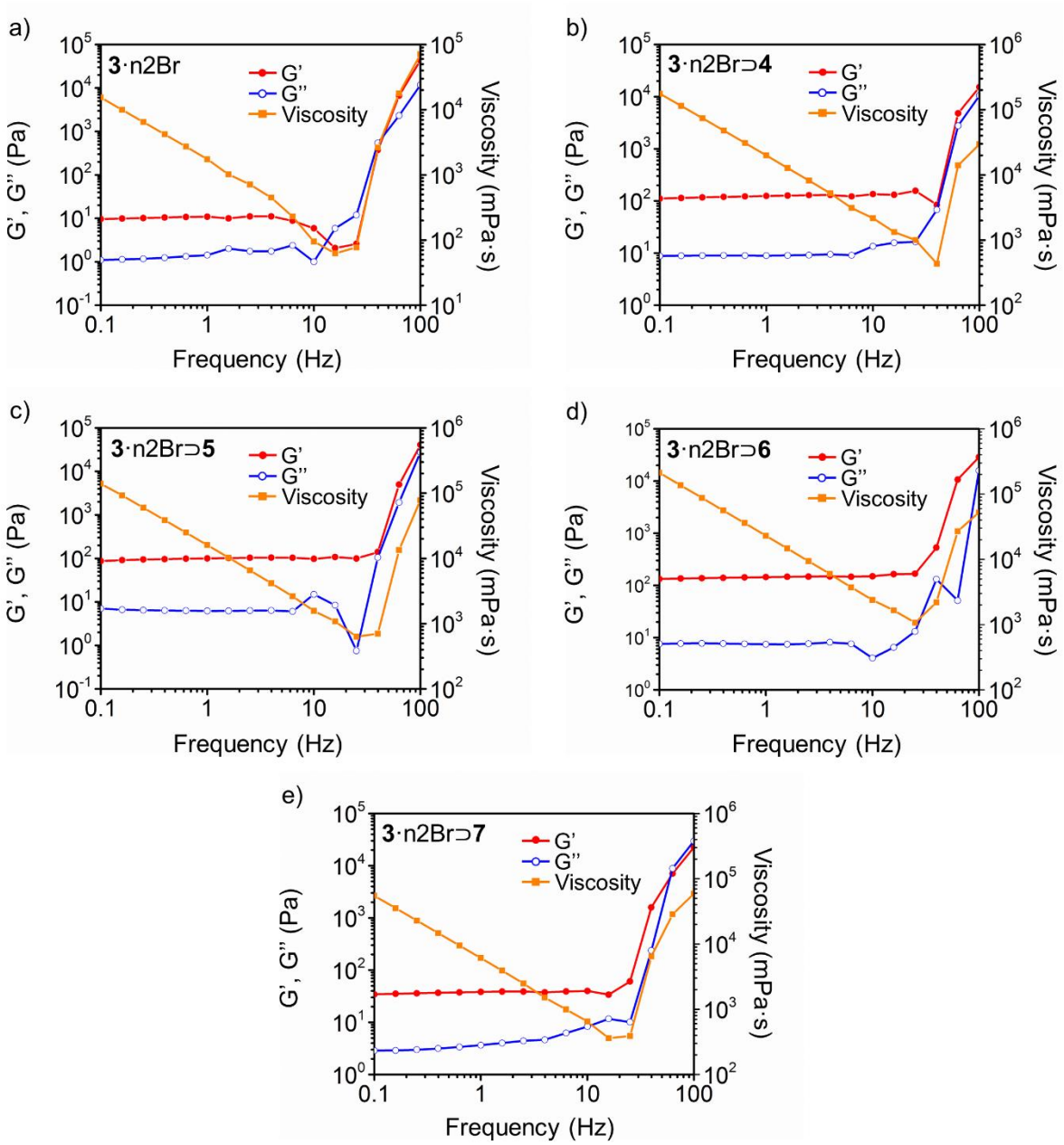

Figure S29. Oscillation frequency sweep plots of the (a) untemplated and (b-e) templated hydrogels of **3**·n2Br prepared using a monomer concentration of 8 mM.

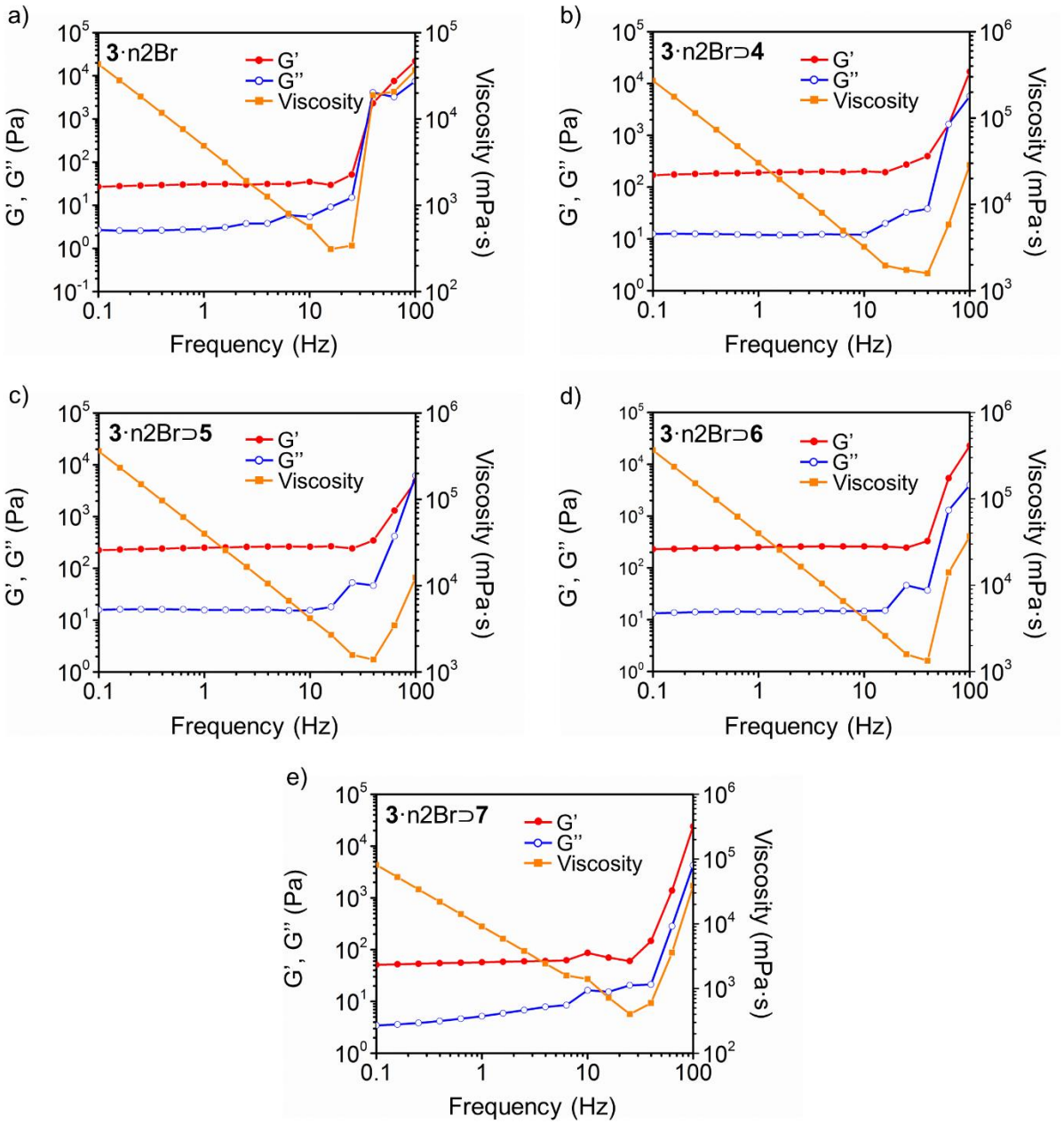

Figure S30. Oscillation frequency sweep plots of the (a) untemplated and (b-e) templated hydrogels of **3**·n2Br prepared using a monomer concentration of 10 mM.

7.3 Viscosity versus Shear Rate Profile Plots

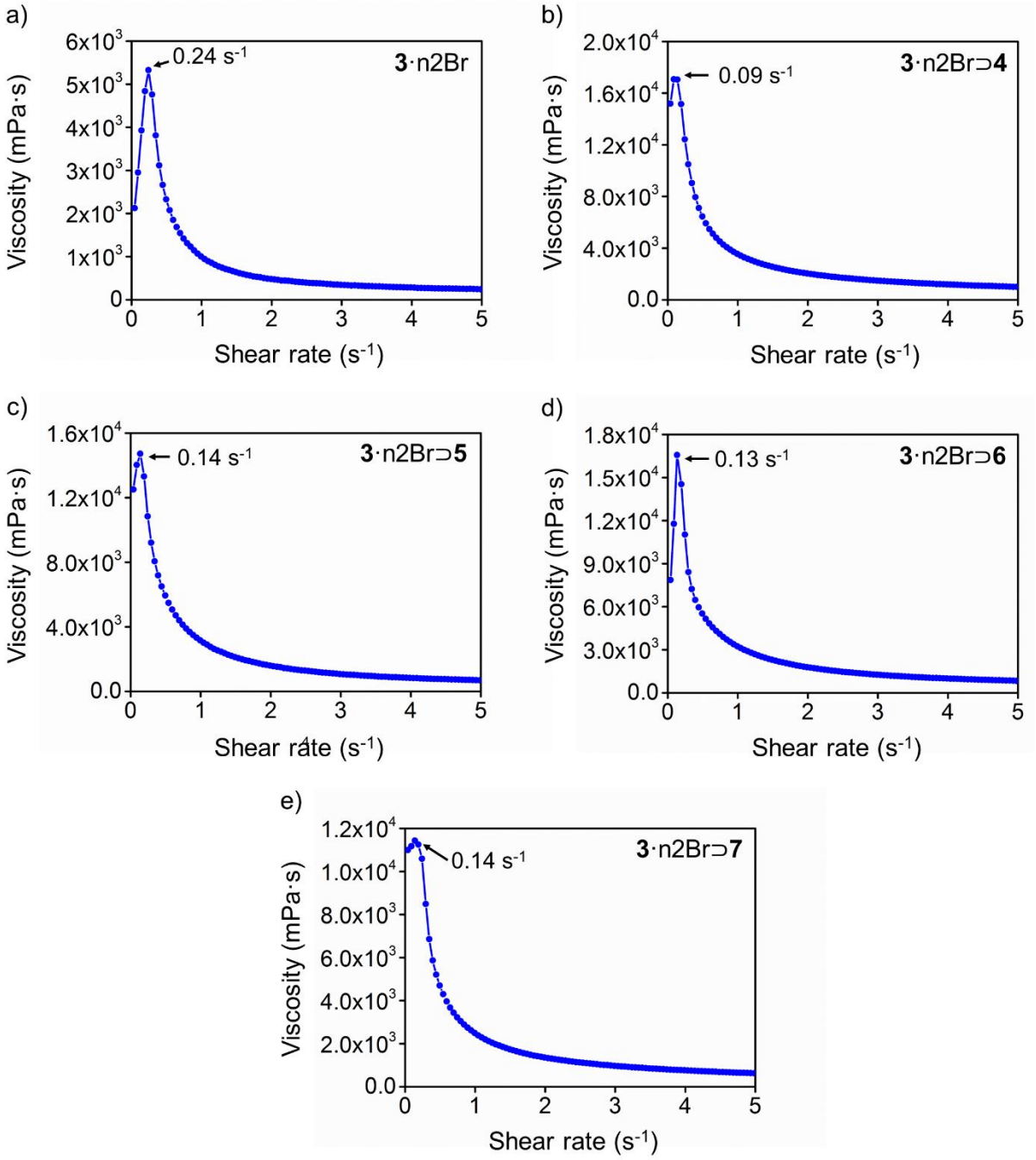

Figure S31. Viscosity versus shear rate profile plots of the (a) untemplated and (b-e) templated hydrogels of **3**·n2Br prepared using a monomer concentration of 4 mM.

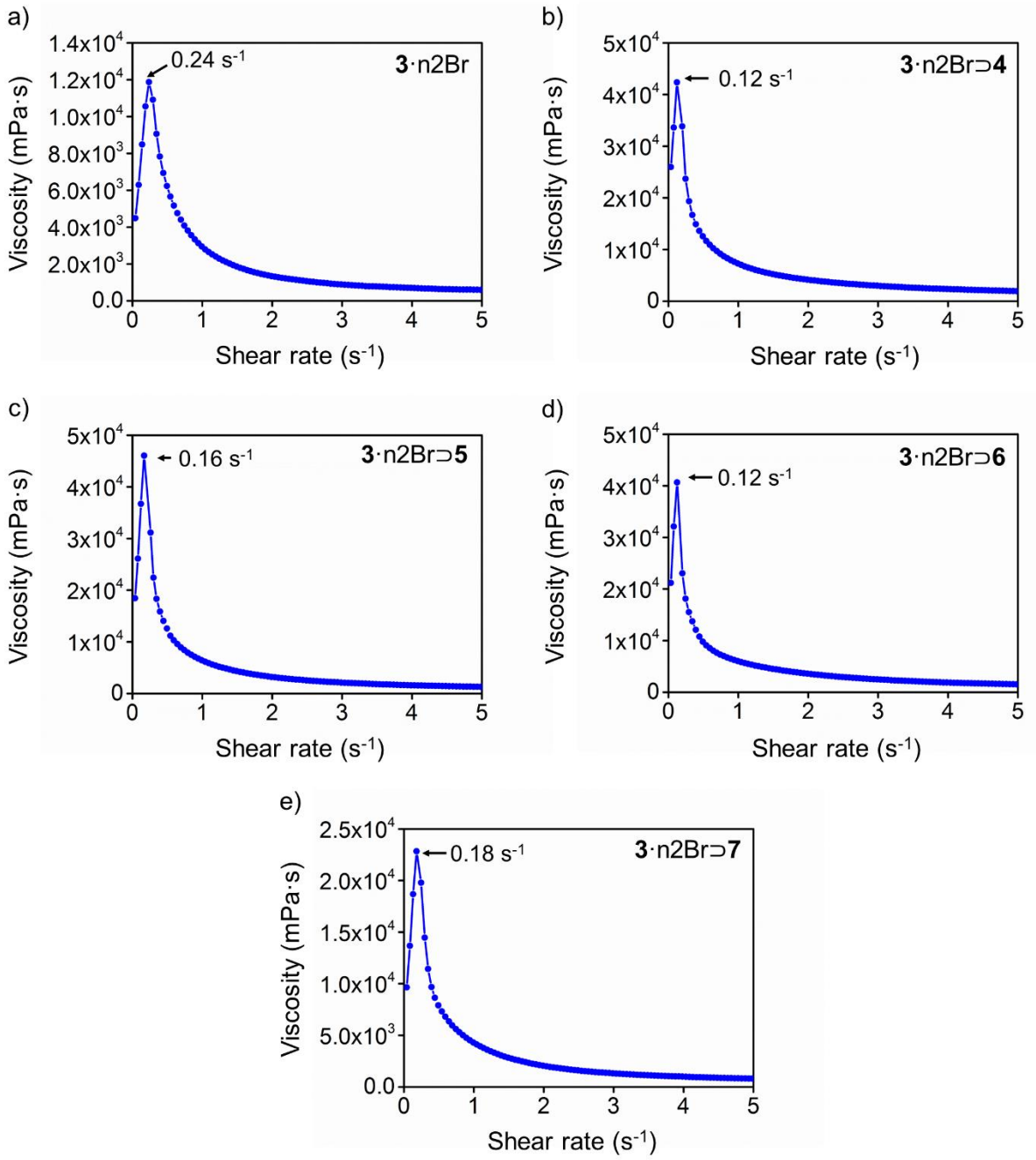

Figure S32. Viscosity versus shear rate profile plots of the (a) untemplated and (b-e) templated hydrogels of **3**·n2Br prepared using a monomer concentration of 6 mM.

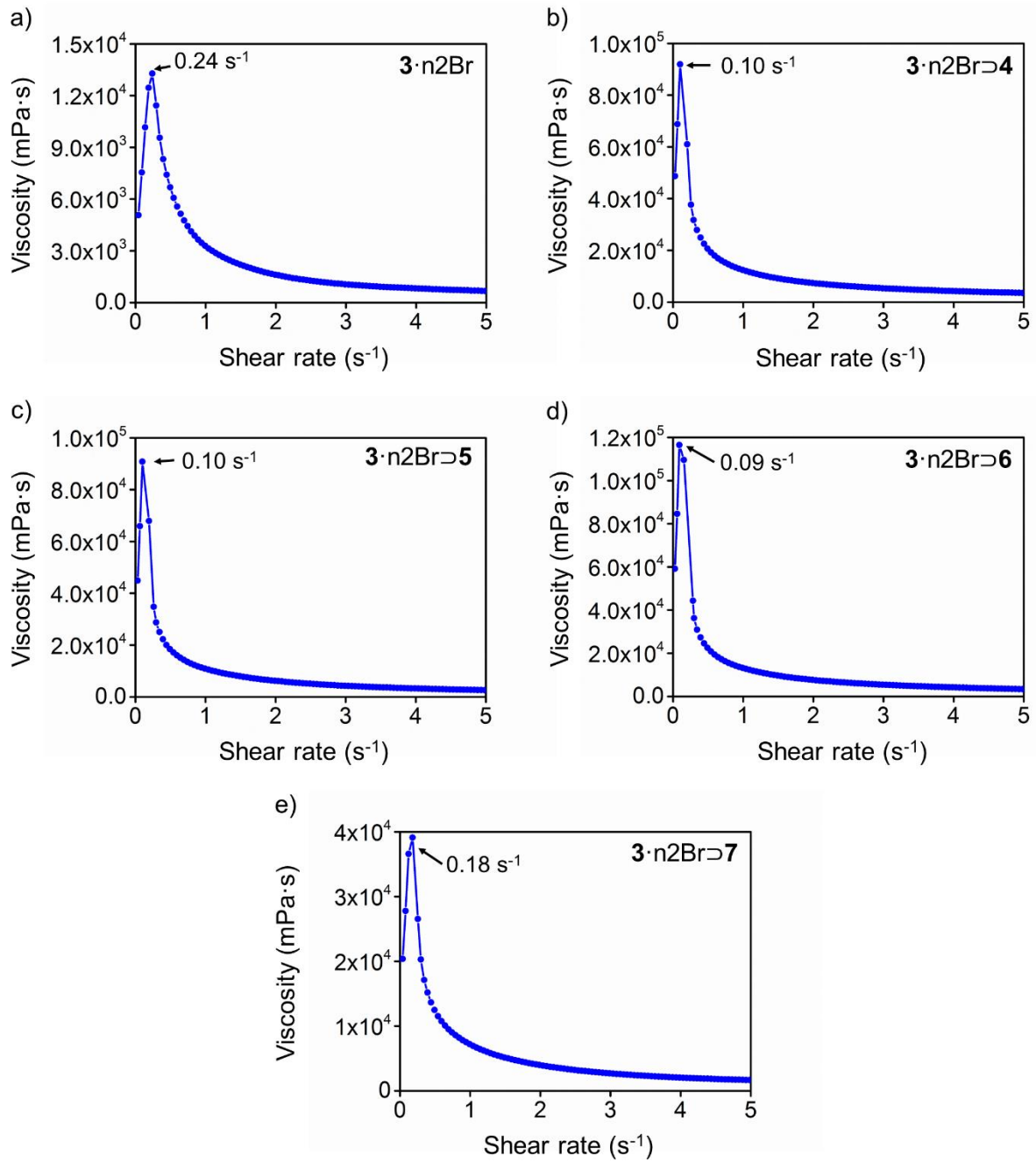

Figure S33. Viscosity versus shear rate profile plots of the (a) untemplated and (b-e) templated hydrogels of **3**·n2Br prepared using a monomer concentration of 8 mM.

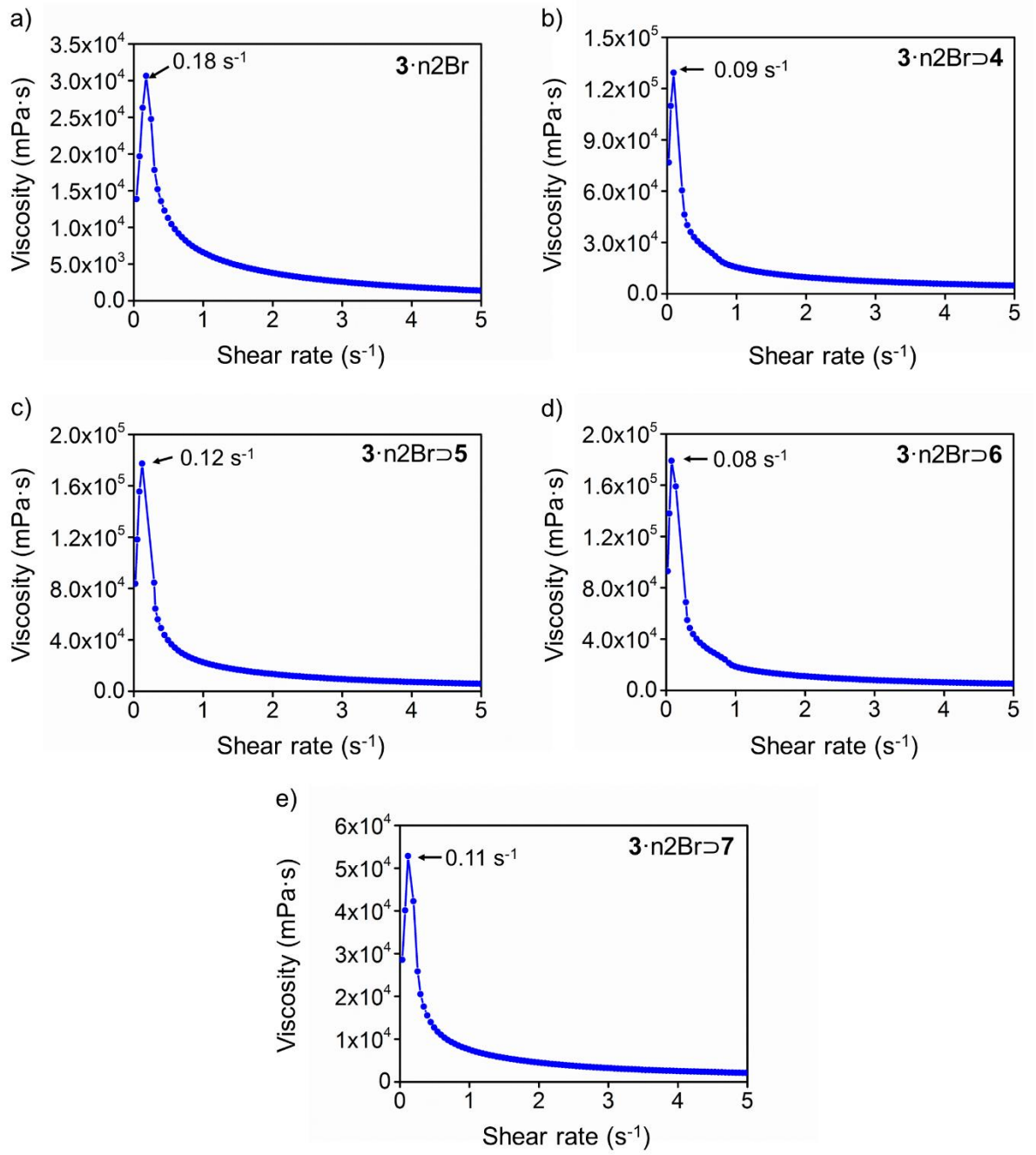

Figure S34. Viscosity versus shear rate profile plots of the (a) untemplated and (b-e) templated hydrogels of **3**·n2Br prepared using a monomer concentration of 10 mM.

7.4 Thixotropic Flow Hysteresis Plots

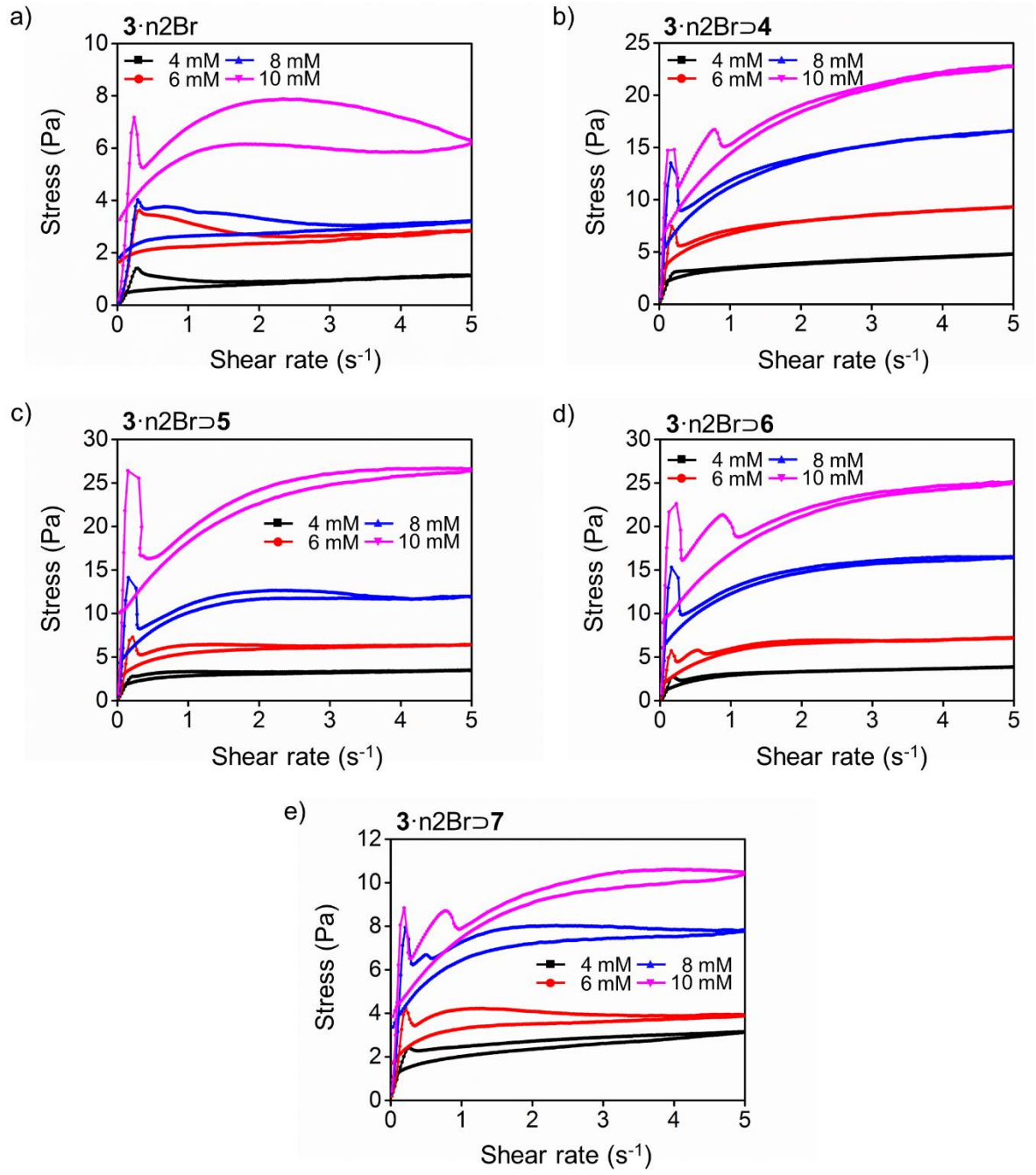

Figure S35: Thixotropic flow hysteresis curves of the (a) untemplated and (b-e) templated hydrogels of **3**·n2Br prepared using monomer concentrations of 4, 6, 8, and 10 mM.

Table S2. Rheological Yield Point ($T_{y)}$, Flow Point ($T_{f)}$, Viscosity, and Relative Thixotropic Area ($S_{R)}$ Measured for **3**·n2Br-based hydrogels in the Absence and Presence of Molecular Templates at 298 K

Protocol[a]	T_y[b] (Pa)	T_f[c] (Pa)	Viscosity[d] (mPa·s)	S_r[e] (%)
4 mM				
No Template	1.42	3.31	710	13.3
Template **4**	0.63	4.99	5468	2.6
Template **5**	0.33	4.63	5824	6.5
Template **6**	1.78	3.71	2644	2.1
Template **7**	0.18	3.70	4921	11.2
6 mM				
No Template	1.09	6.99	1527	12.7
Template **4**	1.35	8.49	10797	1.6
Template **5**	1.77	8.34	6846	6.9
Template **6**	1.80	6.01	7188	4.4
Template **7**	1.16	6.44	3189	11.5
8 mM				
No Template	1.09	6.31	1744	13.2
Template **4**	3.58	13.27	19906	2.8
Template **5**	6.83	12.87	16025	7.0
Template **6**	6.63	16.03	23031	4.1
Template **7**	2.77	10.21	6101	8.3
10 mM				
No Template	1.96	9.26	4901	17.9
Template **4**	6.89	15.02	30380	4.7
Template **5**	10.19	21.33	40000	8.0
Template **6**	11.30	21.34	39940	6.9
Template **7**	5.85	11.22	9117	7.4

[a]Concentrations refer to the starting monomer concentration with a template equivalent of 1:1 per bipyridinium unit. [b]Yield point is defined as 5% deviation in G' from the linear viscoelastic region in accordance with the standards of the International Organization for Standardization (ISO 6721-10). [c]Flow point is defined as the crossover point where G'=G''. [d]Viscosity at 1 Hz obtained from oscillation frequency sweep experiments. [e]Obtained from thixotropic flow hysteresis curves

8 Multi-Point BET Plots and N_2 Adsorption Isotherms at 77 K

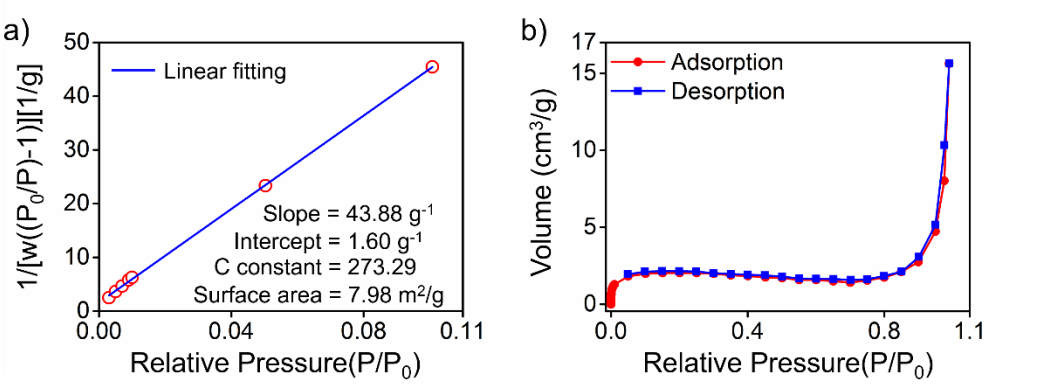

Figure S36: Multi-Point BET plot and N_2 adsorption isotherm of aerogel **3**·n2Br at 77 K

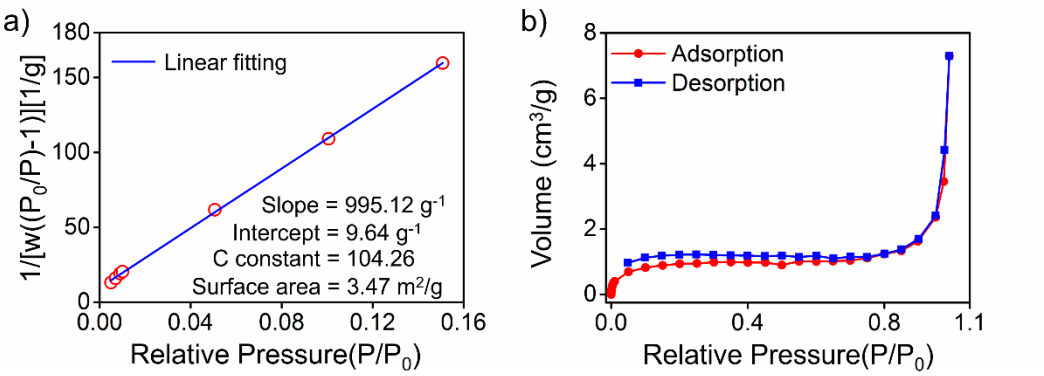

Figure S37: Multi-Point BET plot and N_2 adsorption isotherm of aerogel **3**·n2Br⊃**4** at 77 K

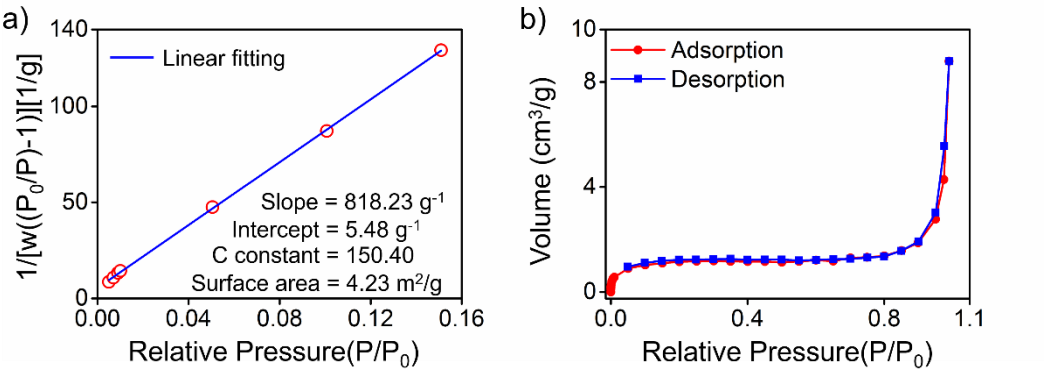

Figure S38: Multi-Point BET plot and N_2 adsorption isotherm of aerogel **3**·n2Br⊃**5** at 77 K

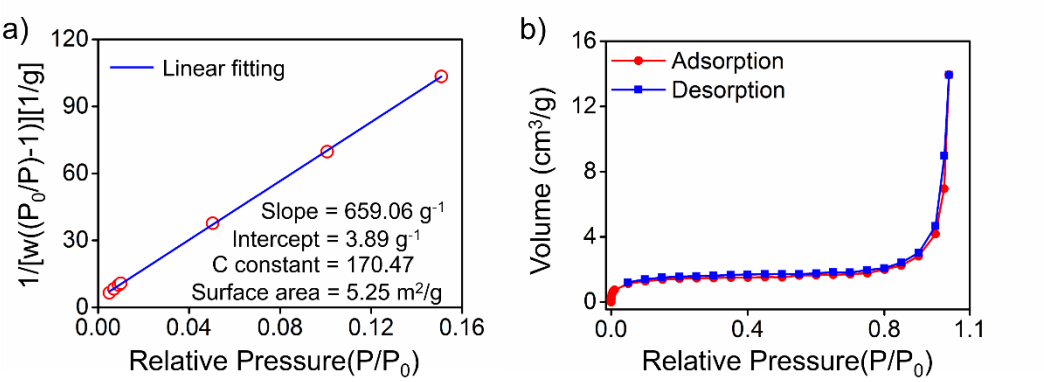

Figure S39: Multi-Point BET plot and N_2 adsorption isotherm of aerogel **3**·n2Br⊃**6** at 77 K

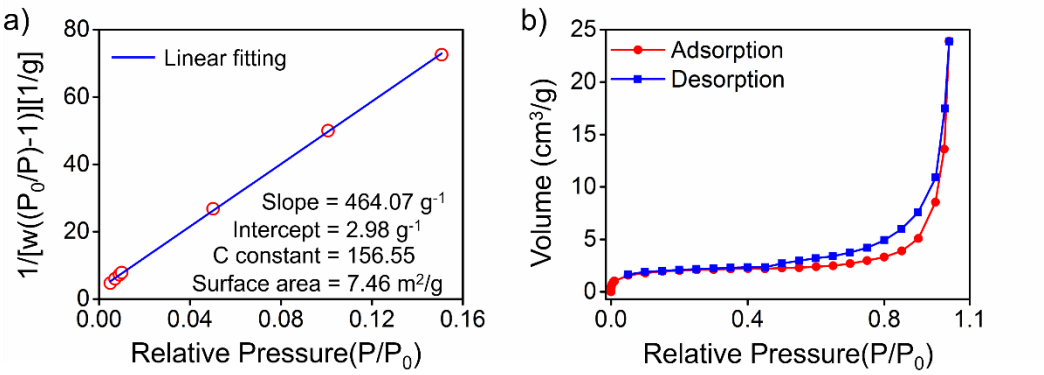

Figure S40: Multi-Point BET plot and N_2 adsorption isotherm of aerogel **3**·n2Br⊃**7** at 77 K

9. XPS Analysis of Iodine-Loaded Aerogels

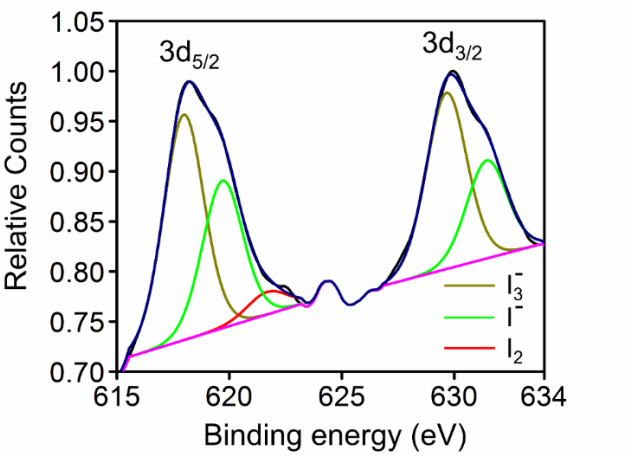

Figure S41: XPS analysis of iodine-loaded aerogel **3**·n2Br

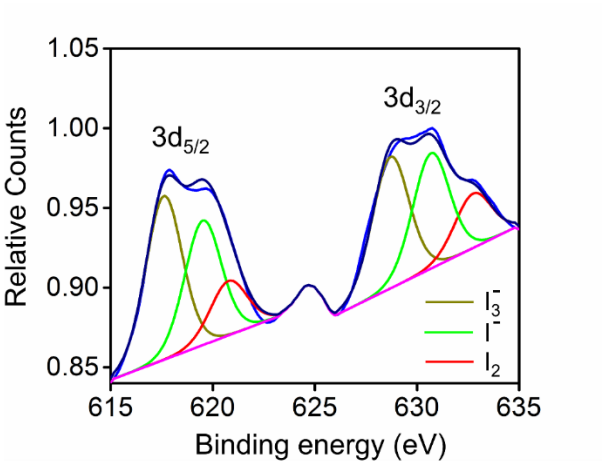

Figure S42: XPS analysis of iodine-loaded aerogel **3**·n2Br⊃**4**

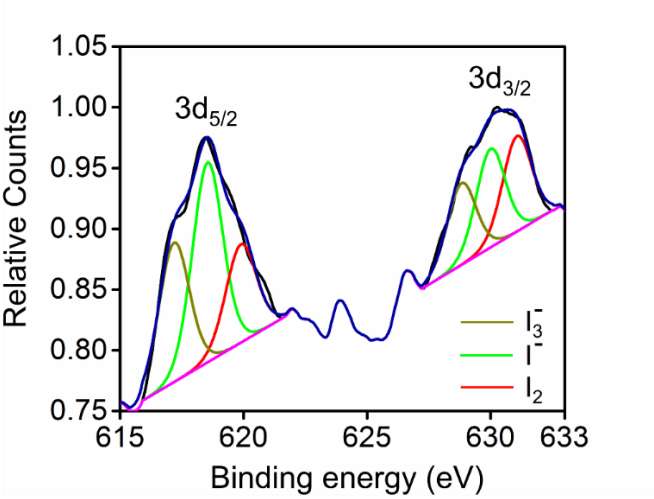

Figure S43: XPS analysis of iodine-loaded aerogel **3**·n2Br⊃**5**.

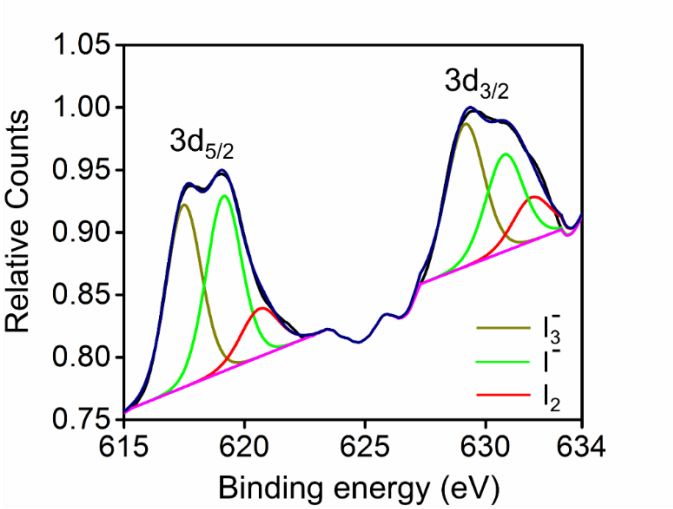

Figure S44: XPS analysis of iodine-loaded aerogel **3**·n2Br⊃**6**.

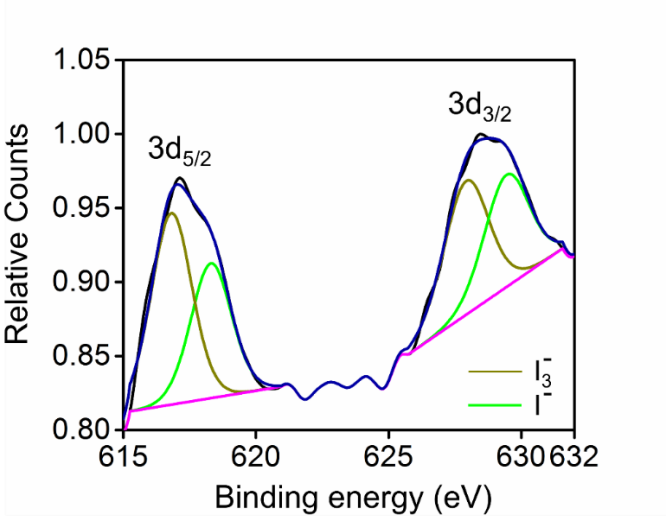

Figure S45: XPS analysis of iodine-loaded aerogel **3**·n2Br⊃**7**.

10. Time-Dependent Removal Efficiency of Iodine in Cyclohexane

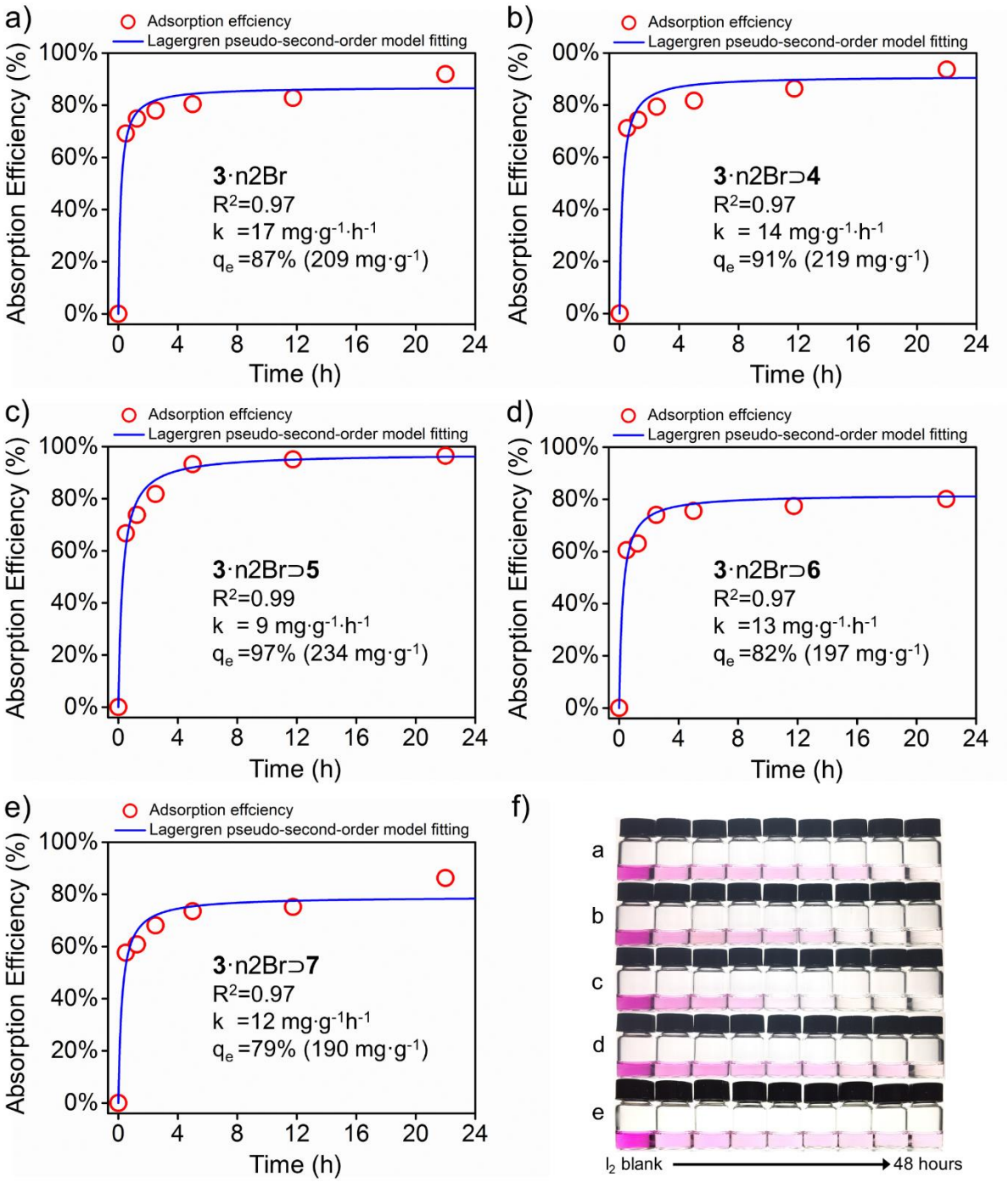

Figure S46: Kinetic analysis and visual detection of iodine removal in cyclohexane solution of I_2 (300 mg/mL) of 5 mg of aerogels a-e **3**·n2Br**, 3**·n2Br⊃**4, 3**·n2Br⊃**5, 3**·n2Br⊃**6, 3**·n2Br ⊃**7**, respectively. f. Visual detection of iodine removal from cyclohexane solution of I_2 of aerogels.

11. Comparison of Iodine Capture with Reported Materials

Table S3: Comparison of Uptake of Gaseous or Dissolved Iodine with Reported Materials

Sample	Iodine Sorption Method	Time taken for I2 Adsorption	Temperature (K)	Iodine Uptake (wt%) (% removal)	Reference
3·n2Br	Vapor adsorption/Cyclohexane	70 h (Vapor) 48 h (Cyclohexane)	293	200 87	This Work
3·n2Br⊃**4**	Vapor adsorption/Cyclohexane	70 h (Vapor) 48 h (Cyclohexane)	293	210 91	This Work
3·n2Br⊃**5**	Vapor adsorption/Cyclohexane	70 h (Vapor) 48 h (Cyclohexane)	293	363 97	This Work
3·n2Br⊃**6**	Vapor adsorption/Cyclohexane	70 h (Vapor) 48 h (Cyclohexane)	293	343 82	This Work
3·n2Br⊃**7**	Vapor adsorption/Cyclohexane	70 h (Vapor) 48 h (Cyclohexane)	293	296 79	This Work
PAF-1	Fixed vapor pressure	10 h (In n-hexane)	333	74.2	1
JUC-Z2	Vacuum swing adsorption	10 h (in n-hexane)	298	59.0	1
JUC-Z2	Fixed vapor pressure	10 h (in n-hexane)	333	80.4	1
{[Zn3(DLlac)2(pybz2)]·2.5DMF}n	Vapor adsorption/Cyclohexane	90 min (Vapor) 48 h (Cyclohexane)	-	82.6	2
PAF-23	Vapor adsorption/Cyclohexane	48 h (Vapor) 72 h (Cyclohexane)	348	271	3
PAF-24	Vapor adsorption/Cyclohexane	48 h (Vapor) 72 h (Cyclohexane)	348	276	3
PAF-25	Vapor adsorption/Cyclohexane	48 h (Vapor) 72 h (Cyclohexane)	348	260	3

Azo-Trip	Vapor adsorption/Cyclohexane	48 h (Vapor) 36 h (Cyclohexane	350	233	4
NiP-CMP	Vapor adsorption/Cyclohexane	48 h (Vapor) 24 h (Cyclohexane)	350	202	5
$[Mo_3S_{13}]$	Vapor adsorption	24 h	333	100	6
$Sb_4Sn_3S_{12}$, Zn_2SnS_6, and $K_{0.1}6CoS_x$	Vapor adsorption	48 h	348	225	7
$(BEA)_2[PbBr_4]$	Vapor adsorption	4-72 h	313	43	8
COP_1^{++}	Vapor adsorption/Cyclohexane	3 min (Vapor)	333	212	9
$COP_1^{\bullet+}$	Vapor adsorption/Cyclohexane	3 min (Vapor)	333	195	9
COP_1^{0}	Vapor adsorption/Cyclohexane	3 min (Vapor)	333	380	9
COP_2^{++}	Vapor adsorption/Cyclohexane	3 min (Vapor)	333	258	9
$COP_2^{\bullet+}$	Vapor adsorption/Cyclohexane	3 min (Vapor)	333	211	9
COP_2^{0}	Vapor adsorption/Cyclohexane	3 min (Vapor)	333	277	9
Pyrrolidinone-based HCPs	Vapor adsorption	12 h	348	460	10
Viologen-based HCPs-V2	Vapor adsorption	60 h	348	525	11
PEI-impregnated-HCPs	Vapor adsorption	10 h	348	607	12
PSIF-1a	Vapor adsorption	15 h	348	542	13
PSIF-2a	Vapor adsorption	15 h	348	575	*13*
PSIF-3a	Vapor adsorption	15 h	348	501	*13*
PSIF-4a	Vapor adsorption	15 h	348	439	*13*
PSIF-5a	Vapor adsorption	15 h	348	534	*13*
COP_1^{++}	Vapor adsorption	24 h	343	162	14
$COP_1^{\bullet+}$	Vapor adsorption	24 h	343	197	*14*
COP_1^{0}	Vapor adsorption	24 h	343	158	*14*

COP_2^{++}	Vapor adsorption	24 h	343	139	*14*
$COP_2^{\bullet+}$	Vapor adsorption	24 h	343	147	*14*
COP_2^{0}	Vapor adsorption	24 h	343	176	*14*
Graphene sheets	Vapor adsorption	120 h	298	85	15
Mg/Al layered double hydroxide	Vapor adsorption	1-2 days	350	152	16
1,3,4-trikis(4-aminophenyl)benzene-biologen nanosheets	Vapor adsorption	22 h	313	145	17
Pyrene-and viologen-based nanosheets	Vapor adsorption			61	18

12. References

1. C. Pei, T. Ben, S. Xua and S. Qiu, *J. Mater. Chem. A*, **2014**, *2*, 7179–7187.
2. M.-H. Zeng, Q.-X. Wang, Y.-X. Tan, S. Hu, H.-X. Zhao, L.-S. Long and M. Kurmoo, *J. Am. Chem. Soc.*, **2010**, *132*, 2561–2563.
3. Z. Yan, Y. Yuan, Y. Tian, D. Zhang and G. Zhu, *Angew. Chem. Int. Ed.*, **2015**, *54*, 12733–12737.
4. Q.-Q. Dang, X.-M. Wang, Y.-F. Zhan and X.-M. Zhang, *Polym. Chem.*, **2016**, *7*, 643–647
5. S. A, Y. Zhang, Z. Li, H. Xia, M. Xue, X. Liu and Y. Mu, *Chem. Commun.*, **2014**, *50*, 8495–8498.
6. K. S. Subrahmanyam, C. D. Malliakas, D. Sarma, G. S. Armatas, J. Wu and M. G. Kanatzidis, *J. Am. Chem. Soc.*, **2015**, *137*, 13943–13948.
7. K. S. Subrahmanyam, D. Sarma, C. D. Malliakas, K. Polychronopoulou, B. J. Riley, D. A. Pierce, J. Chun and M. G. Kanatzidis, *Chem. Mater.*, **2015**, *27*, 2619–2626.
8. D. D. Solis-Ibarra and H. I. Karunadasa, *Angew. chem. Int. Ed.*, **2014**, *53*, 1039–1042.

9. G. Das, T. Prakasam, S. Nuryyeva, D. S. Han, A. Abdel-Wahab, J.-C. Olsen, K. Polychronopoulou, C. Platas-Iglesias, F. Ravaux, M. Jouiad and A. Trabolsi, *J. Mater. Chem. A*, **2016**, *4*, 15361–15369
10. X. Li, G. Chen, J. Ma and Q. Jia, *Sep. Purif. Technol.*, **2019**, *210*, 995–1000.
11. X. Li, G. Chen and Q. Jia, *Micropor. Mesopor. Mater.*, **2019**, *279*, 186–192.
12. X. Li, G. Chen and Q. Jia, *J. Taiwan Inst Chem. E*, **2018**, *93*, 660–666.
13. M. Janeta, W. Bury and S. Szafert, *ACS Appl. Mater. Interfaces*, **2018**, *10*, 19964–19973.
14. T. Skorjanc, D. Shetty, S. K. Sharma, J. Raya, H. Traboulsi, D. S. Han, J. Lalla, R. Newlon, R. Jagannathan, S. Kirmizialtin, J. C. Olsen and A. Trabolsi, *Chem. Eur. J.*, **2018**, *24*, 8648–8655.
15. S. M. Scott, T. Hu, T. Yao, G. Xin and J. Lian, *Carbon N. Y.*, **2015**, *90*, 1-8.
16. S. Ma, S. M. Islam, Y. Shim, Q. Gu, P. Wang, H. Li, G. Sun, X. Yang and M. G. Kanatzidis, *Chem. Mater.*, **2014**, *26*, 7114–7123.
17. G. Das, T. Skorjanc, S. K. Sharma, F. Gándara, M. Lus, D. S. S. Rao, S. Vimala, S. K. Prasad, J. Raya, D. S. Han, R. Jagannathan, J.-C. Olsen and A. Trabolsi, *J. Am. Chem. Soc.*, **2017**, *139*, 9558–9565.
18. G. Das, T. Skorjanc, S. K. Sharma, T. Prakasam, C. Platas-Iglesias, D. S. Han, J. Raya, J. C. Olsen, R. Jagannathan and A. Trabolsi, *ChemNanoMat*, **2018**, *4*, 61–65.